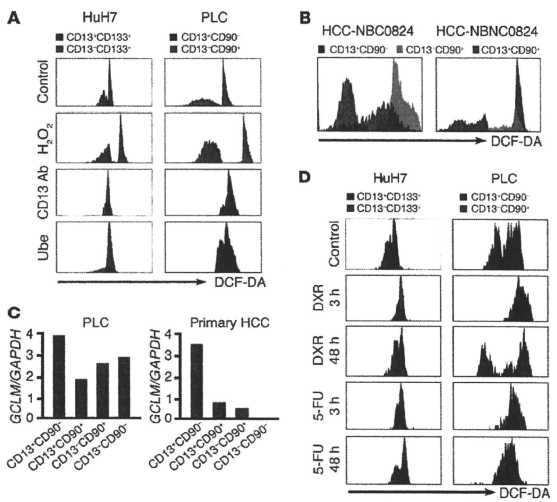

Figure 7

$CD13^+$ cells contain lower levels of ROS than $CD13^-$ cells. (**A**) The expression of prooxidant DCF-DA in $CD13^+CD133^+$ and $CD13^-CD133^+$ HuH7 cells and $CD13^+CD90^-$ and $CD13^-CD90^+$ PLC/PRF/5 cells. Controls, treated with 10 μg/ml of mouse anti-human IgG. As positive controls, cells were treated with 100 μM of oxidant H_2O_2 for 2 hours. Cells were treated with 5 μg/ml of CD13-neutralizing antibody and 25 μg/ml of ubenimex for 4 hours. (**B**) The expression of ROS in the $CD13^+CD90^-$, $CD13^-CD90^+$, and $CD13^+CD90^+$ fractions of 2 clinical HCC samples. (**C**) The expression of the ROS scavenger pathway gene *GCLM* in isolated $CD13^+CD90^-$, $CD13^+CD90^+$, $CD13^-CD90^+$, and $CD13^-CD90^-$ cells from PLC/PRF/5 and clinical HCC samples estimated by semiquantitative RT-PCR. (**D**) The time-course change of ROS expression in DXR or 5-FU treatment. Cells were treated with 1 μg/ml of DXR and 1 μg/ml of 5-FU continuously. After 3 hours and 48 hours of treatment, ROS levels in each population were measured.

with ubenimex plus 5-FU, there were numerous DNA fragments in residual tumor cells (Figure 6B).

After 14 days of treatment, the tumor volume was significantly decreased in the ubenimex-plus-5-FU groups compared with the control and 5-FU or ubenimex groups (Figure 6, C and D).

Next, we studied the effects of CD13 inhibition as it pertains to the self-renewing ability of cells and repopulation of tumors. The $CD13^+$-enriched fraction obtained from 5-FU-treated mice was serially transplanted into secondary NOD/SCID mice. Starting the day after transplantation, the mice were treated with ubenimex (20 mg/kg) for 7 days. After 3 weeks, no tumor formation was observed in the ubenimex-treated mice ($n = 0/6$), whereas 60% of the untreated mice grew tumors ($n = 6/10$) (Figure 6E).

The $CD13^+$ HCC cells contain lower levels of ROS. We focused on the ROS scavenger pathway to determine why DNA fragmentation and apoptosis were induced by CD13 inhibition. It has been reported that self-renewing dormant stem cells normally possess low levels of intracellular ROS and that deregulation of ROS levels impairs stem cell functions (27). Intracellular ROS levels were measured by prooxidants using the 2′,7′-dichlorofluorescein diacetate (DCF-DA) stain. Both in HuH7 and PLC/PRF/5, the $CD13^+$ fraction contained lower concentrations of ROS than the $CD133^{strong}$ and $CD90^+$ fractions. After stimulation of oxidative stress by H_2O_2, a lower concentration of ROS was clearly observed in the $CD13^+$ fraction compared with the $CD13^-$ fraction. Following treatment with the CD13-neutralizing antibody or ubenimex, the ROS concentration was significantly increased in $CD13^+$ cells and reached the level of ROS observed in the $CD13^-$ fraction (Figure 7A). In clinical HCC samples, the results were similar to those in PLC/PRF/5, as the $CD13^+CD90^-$ fraction exhibited lower ROS levels than those in the $CD13^-CD90^+$ and $CD13^+CD90^+$ fractions (Figure 7B). The $CD13^+$ fraction also contained another ROS indicator, MitoSOX (a highly selective marker for mitochondrial superoxide), which was markedly lower in the PLC and clinical HCC samples and less in HuH7 (Supplemental Figure 6).

To study the correlation between CD13 and the ROS scavenger pathway, the expression of *Gclm* was assessed by RT-PCR. *Gclm* encodes the glutamate-cysteine ligase that catalyses the rate-limiting synthesis step of glutathione (GSH), which works as a critical cellular reducing agent and anti-oxidant. *Gclm* was overexpressed in the $CD13^+CD90^-$ fraction ($P < 0.001$) compared with the $CD13^+CD90^+$, $CD13^-CD90^+$, and $CD13^-CD90^-$ fractions in PLC/PRF/5 and primary HCC cells (Figure 7C).

It is well known that cell destruction after exposure to cytotoxic chemotherapy and ionizing radiation is partially due to free radicals (28, 29). Given that the present study indicates a low ROS concentration in the $CD13^+$ population, we were interested to see whether chemotherapy agents actually increase ROS level of $CD13^+$ population. To study this, ROS levels of $CD13^+CD133^+$ and $CD13^-CD133^+$ populations in HuH7, and $CD13^+CD90^-$ and $CD13^-CD90^+$ populations in PLC/PRF/5 were measured 3 hours and 48 hours after of DXR or 5-FU treatment. After 3 hours treatment with DXR, ROS levels were increased in both $CD13^+$ and $CD13^-$ populations in HuH7 and PLC/PRF/5. Interestingly, after 48-hour treatment with DXR, ROS levels of $CD13^+$ populations were decreased and reached those of control levels. Especially in PLC/PRF/5, $CD13^+CD90^-$ populations showed 2 peaks of ROS levels, one of which contained further lowered ROS levels than control. With 5-FU treatment, though the power of upregulation of ROS levels was weaker than those of DXR, ROS levels of $CD13^+$ fractions were actually increased to those of $CD13^-$ fractions. As with the data regarding DXR treatment, after 48 hours of 5-FU treatment, $CD13^+$ populations showed lower levels of ROS compared with those of the $CD13^-$ population (Figure 7D). These data

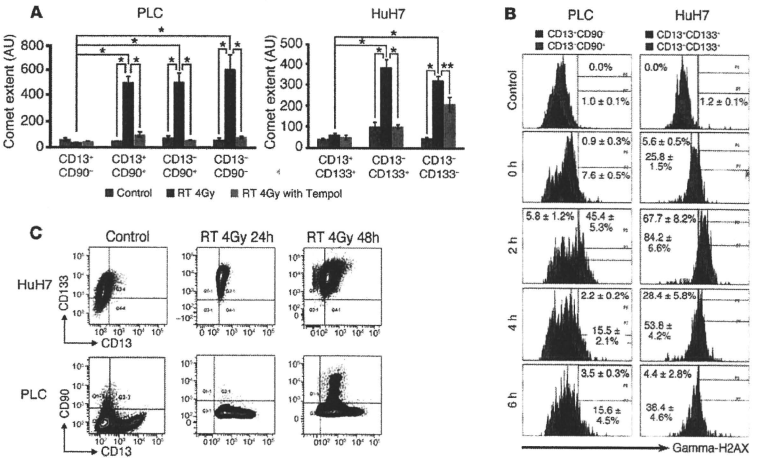

Figure 8

High levels of ROS scavenger expression parallel DNA damage in CD13⁺ HCC cells. (**A**) Isolated cell fractions of CD13⁺CD90⁻, CD13⁺CD90⁺, CD13⁻CD90⁺, and CD13⁻CD90⁻ in PLC/PRF/5 and CD13⁺CD133⁺, CD13⁻CD133⁺, and CD13⁻CD133⁻ in HuH7 were irradiated with 4 Gy with or without antioxidant tempol. Data show the tail lengths in the alkaline comet assay of control (blue), 4 Gy irradiation (brown), and antioxidant tempol pretreated (green) cells. *$P < 0.01$. **NS. (**B**) HuH7 and PLC/PRF/5 cells were irradiated with 4 Gy, and time course change of gamma-H2AX expression in each population was assessed. Numbers indicate the percentage of gamma-H2AX in CD13⁺CD90⁻ PLC/PRF/5 and CD13⁺CD133⁺ HuH7 cells (red) and CD13⁻CD90⁺ PLC/PRF/5 and CD13⁻CD133⁺ HuH7 cells (blue) with ± SD. (**C**) HuH7 and PLC/PRF/5 cells were irradiated with 4 Gy, seeded in culture medium, and their expressions analyzed after 24 and 48 hours. Damaged and dead cells were eliminated with 7-AAD. The cut-off lines were determined using isotype controls.

together with the observation that CD13⁺ cells remained after treatment with chemotherapy agents (Figure 4A), suggest that ROS levels of all of the cells are temporally upregulated when cells are treated with chemotherapy agents and that this leads to disruption of the CD13⁻ population, whereas in the CD13⁺ cells, ROS levels are downregulated by the ROS scavenger pathway and the cells survive. In addition, proliferative CD13⁻ cells are easily affected by the DNA synthesis inhibition effect of chemotherapy agents.

To assess radiation-induced DNA damage with ROS, purified CD13⁺CD90⁻, CD13⁺CD90⁺, CD13⁻CD90⁺, and CD13⁻CD90⁻ PLC/PRF/5 cells were irradiated and subjected to an alkaline comet assay. Although untreated cells did not show significantly different levels of DNA damage, there were fewer DNA strand breaks in CD13⁺CD90⁻ cells than in the other 3 fractions ($P < 0.01$) after ionizing irradiation. The DNA damage in these 3 fractions (but not in the CD13⁺CD90⁻ fraction) was significantly inhibited ($P < 0.001$) by treatment with an antioxidant reagent, tempol (Figure 8A). In HuH7 cells, the CD13⁺ fraction also exhibited lower levels of DNA damage compared with the CD13⁻ fraction. There was no significant difference between the irradiated and tempol-treated groups for the CD13⁻CD133⁻ fraction (Figure 8A). These findings reveal that the enhanced ROS defenses in the CD13⁺ fraction contribute to the reduction in DNA damage after genotoxic cancer therapy. To confirm radiation-induced DNA double-strand break status in CD13⁺ and CD13⁻ populations, time-course change of gamma-H2AX, a marker of double-strand breaks (30), was studied. In PLC/PRF/5, after 4 Gy of irradiation, gamma-H2AX expression in CD13⁻CD90⁺ population increased after 2 hours of irradiation (45.4% ± 5.3%) and then decreased within 6 hours (15.6% ± 4.5%), whereas gamma-H2AX expression in CD13⁺CD90⁻ population did not. In HuH7, gamma-H2AX expression increased after 2 hours in both CD13⁺CD133⁺ and CD13⁻CD133⁺ populations and decreased rapidly in the CD13⁺CD133⁺ population (4.4% ± 2.8%) compared with the CD13⁻CD133⁺ population (38.4% ± 4.6%) (Figure 8B). After 24 hours of irradiation, the residual cells were localized in the CD13⁺ fraction in HuH7 and in the CD13⁺CD90⁻ fraction in PLC/PRF/5 (Figure 8C). Although there were some different manners in time-course change of gamma-H2AX in PLC/PRF/5 and HuH7, surviving cells after 24 hours of irradiation were localized in the CD13⁺ population, suggesting the radio-resistant characteristics of the CD13⁺ population, due to rapid recovery of DNA damage. After 48 hours of irradiation, the residual cells began to proliferate and produced CD13⁻CD133⁺ cells in HuH7 and CD13⁺CD90⁺ cells in PLC/PRF/5 (Figure 8C). These studies support the time-course studies (Figure 3C) and indicate that CD13⁺ cells exist as a core fraction in the cellular hierarchy.

Discussion

To achieve the goal of a radical cure for cancer, recurrence and metastasis caused by residual cancer cells are barriers that need to

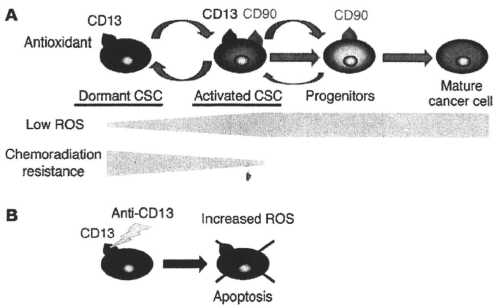

Figure 9
The CD13⁺ CSCs of the liver generate genotoxic resistance through reduced levels of ROS (proposed schema). (**A**) Results indicate that CD13⁺CD90⁻ CSCs of the liver are dormant and exhibit reduced intracellular ROS levels and, because of increased antioxidants, may result in resistance to genotoxic chemo/radiation therapy. On the other hand, CD13⁻CD90⁺ CSCs actively proliferate and are sensitive to therapy. (**B**) Neutralization or inhibition of CD13 may result in an increase in intracellular ROS in CD13⁺CD90⁻ CSCs and induction of apoptosis.

be overcome. Recently, the presence of CSCs has attracted attention, and it is thought that these CSCs are intimately involved in cancer recurrence and resistance. In addition, as with leukemia (4, 5), the presence of dormant or slow-growing CSCs is beginning to be recognized in breast cancer (6). However, dormant or slow-growing CSCs have yet to be identified in most solid cancers. In the present study, we identified CD13 as a functional marker that can be used to identify potentially dormant liver CSCs resistant to treatment. Our exploration of SP cells has indicated that CD13⁺ cancer cells are closely associated with SP cells. Cell-cycle studies indicated that CD13⁺ cells exist in lower PY lesions. Cell-fate tracing assay with PKH26GL and immunohistochemical analysis of BrdU-retaining cells demonstrated that CD13⁺ but not CD13⁻ cells exhibited long dye retention and relatively slow proliferation in vitro and in vivo. This population possessed high tumorigenic potential in NOD/SCID mice and also induced chemo resistance. The results of this study are compatible with those of dormancy studies on hematopoietic stem/progenitor (3) and malignant cells (4, 5). CD13, also known as amino peptidase N, is a super family of zinc-binding metalloproteinases that play roles in cellular processes such as mitosis, invasion, cell adhesion, angiogenesis, radiation resistance, and antiapoptosis (31–34). To the best of our knowledge, there have been no reports describing the exclusive expression of CD13 in CSCs of the liver.

The immunohistochemical findings also support the view that CD13⁺ cells play a role in relapse of liver cancer. The apparent increase in the number of CD13⁺ cells near the fibrous capsule after TAE is consistent with the fact that clinical HCC relapse after TAE is frequent at the capsule site (7). These findings are compatible with the results of studies in mouse models that revealed that CD13⁺ cells survived and were amplified after 5-FU treatment. In addition, the preferential accumulation of CD13⁺ HCC cells at the capsule but not in the central region after TAE therapy suggests the attractive hypothesis that cellular components in the fibrous capsule may function as a protective niche (3).

The suppression of CD13 by the CD13-neutralizing antibody or ubenimex showed an effect even if the cancer cells were resistant to the ABC transporter–dependent agent DXR. This finding suggests that CD13⁺ cells have some mechanism of resistance to anticancer agents in addition to their slow growth and ABC transporter (21, 35, 36) expressions. It is known that the control of ROS is indispensable for hematopoietic stem cell maintenance. Oxidative stresses inhibit cellular dormancy and self renewal of hematopoietic stem cells (37, 38). In cancer, low ROS levels and radiation resistance in CD44⁺CD24⁻ breast CSCs has been reported (39). However, an association between ROS and self renewal in CSCs is unknown. In the present study, we demonstrated that CD13⁺ cells contain low levels of ROS. The CD13⁻CD133⁺ and CD90⁺ cells expressed higher levels of the ROS indicators DCF-DA and MitoSOX. RT-PCR of the ROS scavenger pathway gene *GCLM* and a comet assay also indicated that CD13⁺ cells protect themselves from oxidant stress via the ROS pathway. Continuous treatment with anticancer agents predominantly elicits high levels of ROS in the CD13⁻ population. However, in the CD13⁺ population, it elicits low levels of ROS, and these cells survive and are enriched for after chemotherapy. Mice treated with ubenimex exhibited high DNA fragmentation in xenografted tumors. These findings suggest that the ROS scavenger pathway and CD13 are essential to CSC protection and maintenance in the liver (Figure 9, A and B). Importantly, tumorigenicity was completely inhibited by treatment with ubenimex in secondary mice xenografted with a CD13⁺ cell–enriched tumor fraction obtained from 5-FU–treated mice. The suppression of CD13 inhibited self renewal and the tumor-initiation ability of CD13⁺ cells. It is thought that deregulation of ROS pathway may contribute to disruption of CSCs.

The hierarchy analysis of PLC/PRF/5 cells revealed that a small fraction of CD90⁺ cells produce a small number of CD13⁺ cells in vitro. This finding indicates that activated CD90⁺ cells should also be involved in targeted cancer therapy. The CD90⁺ cells were resistant and remained in spite of treatment with ubenimex in vivo. The residual CD90⁺ cells cause cancer regrowth and cancer recurrence by producing tumor-initiating CD13⁺ cells. CD13⁺ cells have high tumorigenicity and self-renewal ability in vivo. But unfortunately, in the case of liver cancer, it is difficult to target the proliferative CD90⁺ cells by using conventional anticancer drugs because some parts of CD90⁺ cells also express CD13. The expression of CD13 is closely related to the multidrug-resistant SP fraction, and CD13 protects cells from apoptosis via the ROS scavenger pathway. Of course, based on CSC concepts, tumors will disappear when CSCs are disrupted completely. This is because the loss of CSCs leads to the destruction of the hierarchical structure within the tumor. However, it may be difficult to obtain complete pharmacokinetic control, especially in vivo. Actually, in this study, we could not achieve complete disappearance of CD13⁺ cells and

could not elicit tumor regression by single agent administration of ubenimex. To overcome these problems, we established combination therapy with ubenimex plus 5-FU to efficiently elicit tumor regression. Ubenimex works to disrupt $CD13^+$ cells by its potential effect of upregulating ROS levels and its inhibition of self-renewal of $CD13^+$ cells. 5-FU inhibits proliferative cancer cells, decreases tumor size, and improves survival. It is known that cell destruction after exposure to cytotoxic chemotherapy and ionizing radiation is partially due to free radicals (29, 39), and it is reported that 5-FU induces ROS in hematopoietic stem cells and suppresses the hematopoietic stem cell niche (40). We have also confirmed that 5-FU works to increase the ROS levels of $CD13^+$ populations. By this combination therapy, tumors were drastically regressed compared with single-agent therapy. It is suggest that 5-FU and ubenimex work in a complementary or additive fashion.

Although the majority of the experiments in this study are based on cell lines, the expression, sphere, and ROS analyses support the contention that PLC/PRF/5 cells reflect clinical HCC and may hold promise for preclinical studies. This study also suggests that the future development of liver cancer therapy based on CSC concepts appears promising. We are attempting to establish human HCC-xenografted preclinical mouse models from clinical HCC samples to provide necessary confirmation of our contention using in vivo assays.

Methods

Cell culture. Human liver cancer cells, HuH7 and PLC/PRF/5, obtained from the Cell Resource Center for Biomedical Research, Institute of Development, Aging, and Cancer (Tohoku University, Sendai, Japan) were cultured in RPMI 1640 (Invitrogen) medium with 10% FBS (Equitech-Bio). Cells were cultured at 37°C in a humidified atmosphere containing 5% CO_2.

Flow cytometric analysis and cell sorting. The antibodies used in this study are listed in Supplemental Table 1. Briefly, cells were harvested with trypsin and EDTA. Doublet cells were eliminated using FSC-A/FSC-H and SSC-A/SSC-H. Dead and damaged cells were eliminated with 7-AAD (BD Biosciences — Pharmingen). Isotype controls (BD Biosciences) were used. FcR blocking was performed using an FcR-blocking reagent (Miltenyi-Biotec). FITC-conjugated anti-human CD45 (BD Biosciences — Pharmingen) and FITC-conjugated Lineage Cocktail (Lin1; BD Biosciences — Pharmingen), which contains antibodies against CD3, CD14, CD16, CD19, CD20, and CD56 and is used to detect lymphocytes, monocytes, eosinophils, and neutrophils, were used for eliminating hematopoietic cells in the clinical sample analysis. For sorting, cells were incubated with 1 μg of each antibody for 30 minutes. Control experiments involved incubation with each antibody for 30 minutes and no apparent increase in the number of dead cells detected by propidium iodide (PI) staining.

Cell-cycle assay. To characterize the SP fractions, 1×10^6 cells in 2% FCS/1 mM HEPES buffer/DMEM were preincubated at 37°C for 30 minutes. Cells were then labeled with 10 μg/ml Hoechst 33342 (Molecular Probes) in staining medium at 37°C for 70 minutes. A total of 15 μg/ml reserpine (Sigma-Aldrich) was used for the Hoechst staining procedure. For cell-cycle analysis by PY staining, cells were first stained with Hoechst 33342 at 37°C. After 50 minutes, 1 μg/ml PY was added and the cells were incubated at 37°C for 20 minutes. FACSVantage SE DiVa (BD) and FACS SORP Aria (BD) were used for analysis and cell sorting. The cell cycle was also studied with 10 μg/ml 7-AAD (BD Biosciences — Pharmingen).

Gene expression study. Total RNA was prepared using TRIzol reagent (Invitrogen). Reverse transcription was performed with SuperScriptIII (Invitrogen). Quantitative real-time RT-PCR was performed using a LightCycler TaqMan Master kit (Roche Diagnostics). The expression of mRNA copies was normalized against *GAPDH* mRNA expression. The PCR primers used for amplification were as follows: *GCLM*, 5′-TGTGTGATGCCACCAGATTT-3′ and 5′-TTCACAATGACCGAATACCG-3′; *GAPDH*, 5′-TTGGTATCGTGGAAGGACTCA-3′ and 5′-TGTCATCATATTTG-GCAGGTTT-3′.

Cell proliferation and chemo-resistance assay. Isolated cells were seeded into 96-well culture plates at 5×10^3 cells/well for cell proliferation assays. After 72 hours, cell viability was determined by an ATP bioluminescence assay (CellTiter-Glo Luminescent Cell Viability Assay; Promega) and the luminescence signal was detected using a luminometer (ARVO MX; Perkin-Elmer) according to the manufacturer's protocol. The cells were seeded onto 96-well culture plates at 5×10^3 cells/well. After 24 hours, DXR was added to the culture medium (0.01, 0.05, and 0.1 μg/ml). After 72 hours of exposure to the chemotherapeutic agent, cell viability was determined using a method similar to that used in the cell proliferation assay.

Cell-fate tracing. Cells were labeled with 20 μM PKH26GL (Sigma-Aldrich) according to the manufacturer's protocol. Purified populations of cells were isolated and seeded onto 4-chamber polystyrene vessel tissue culture-treated glass slides (Falcon; BD Biosciences) at 5×10^3 cells/well. Cells were cultured in RPMI 1640 (Invitrogen) medium with 20% FBS (Equitech-Bio). Cell fate was studied at each 30-minute time point for 238 hours using a time-lapse fluorescence microscope (BZ-9000 Biorevo; KEYENCE). Data were analyzed using a BZ-II analyzer (KEYENCE). BrdU-retaining cells were identified with fresh frozen samples with the modification of using 5-bromo-2′-deoxyuridine Labeling & Detection Kit 1 (Roche Applied Science) and CD13 rabbit polyclonal antibody (Santa Cruz Biotechnology Inc.). As secondary antibody, anti-rabbit IgG Alexa Fluor 555 (Molecular Probes) was used.

Sphere assay. Cells were seeded on ultra-low attachment culture dishes (Corning) in serum-free medium. DMEM/F-12 serum-free medium (Invitrogen) contained 2 mM L-glutamine, 1% sodium pyruvate (Invitrogen), 1% MEM nonessential amino acids (Invitrogen), 1% insulin-transferrin-selenium-X supplement (Invitrogen), 1 μM dexamethasone (Wako), 200 μM L-ascorbic acid 2-phosphate (Sigma-Aldrich), 10 mM nicotinamide (Wako), 100 μg/ml penicillin G, and 100 U/ml streptomycin supplemented with 20 ng/ml epithelial growth factor and 10 ng/ml fibroblast growth factor-2 (PeproTech). Digestion and cell passage were performed every 3 days.

Differentiation assays from spheres. Each single sphere established from normal liver cells was seeded into a culture chamber (BD Biosciences). Spheres were cultured in sphere medium containing 10% FBS to induce the differentiation process. Three days after the spheres became attached to the bottom of the chamber and spreading cells appeared, cells were fixed and stained with anti-human CD13 mouse monoclonal antibody (clone WM15, dilution 1:50; Santa Cruz Biotechnology Inc.), FITC-anti-human albumin goat polyclonal antibody (dilution 1:500; Bethyl Laboratories), anti-human Cytokeratin 19 mouse monoclonal antibody (clone RCK108, dilution 1:50; Dako), and anti-human α-fetoprotein mouse monoclonal antibody (clone 189502, concentration 5 μg/ml; R&D Systems).

Immunohistochemistry. The 4-μm-thick sections were obtained using cryostat and fixed with 4% paraformaldehyde for 15 minutes. After 1 hour of blocking, the sections were incubated overnight at 4°C in a humidified chamber with primary antibodies. For primary antibodies, anti-human CD13 mouse monoclonal antibodies (clone WM15, dilution 1:50; Santa Cruz Biotechnology Inc.), anti-human CA9 rabbit polyclonal antibodies (dilution 1:1000; Novus Biologicals), anti-human CD90 rabbit monoclonal antibodies (dilution 1:1000; Epitomics), and anti-human Ki-67 rabbit polyclonal antibodies (dilution 1:100; Santa Cruz Biotechnology Inc.) were used. For secondary antibodies, goat anti-mouse IgG_1, Alexa Fluor 546–conjugated, and highly cross-adsorbed (Molecular Probes) as well as goat anti-rabbit IgG, Alexa Fluor 488–conjugated and highly cross-adsorbed (Molecular Probes) antibodies were used. The coverslips were mounted using ProLong Gold and SlowFade Gold Antifade Reagent (Molecular

Probes), and the slides were viewed with a fluorescence microscope (BZ-9000 Biorevo). Data were analyzed using BZ-II (Keyence). The continuous cryostat sections were also stained with modified H&E.

Tumor cell preparation. Primary liver cancer samples were obtained from Osaka University with the patients' informed consent and the approval of the Research Ethics Board of Osaka University. Tumor tissues were cut into approximately 2-mm fragments, further minced with a sterile scalpel, and washed twice with DMEM/10% FBS. They were then placed in DMEM/10% FBS with 2 mg/ml collagenase A (Roche Diagnostics) solution. The mixture was incubated at 37°C with shaking until digestion was complete. Cells were filtered through a 40-μm nylon mesh and washed twice and the cell fragments and debris were then eliminated by Ficoll (GE Healthcare) density gradient centrifugation and stained for flow cytometry.

Inhibition of CD13. A total of 5×10^5 cells were seeded into 96-well plates in 200 μl of culture medium. After 24 hours, the medium was replaced with fresh culture medium containing 1, 5, 10, and 20 μg/ml mouse monoclonal anti-human CD13 antibodies (clone WM15; GeneTex) or 25, 50, 100, 250, and 500 μg/ml ubenimex (Nippon Kayaku). Cell viability was assayed at 24, 48, and 72 hours using Cell Counting Kit-8 (Dojindo) according to the manufacturer's instructions. Absorbance was measured at 450 nm using a 680 XR microplate reader (Bio-Rad). A total of 10 ng IgG_1 mouse monoclonal antibody (GeneTex) was used as the negative control. DXR-resistant (DXR-R) HuH7 cells were established by continuous treatment with 1 μg/ml DXR and selection of resistant colonies. Cellular apoptosis was measured using PI and APC–annexin V (BD Pharmingen) with an Apoptosis Detection Kit (BioVision).

In vivo assay. The xenografted mouse model was created by injection of 1×10^5 HuH7 and PLC/PRF/5 cells into NOD/SCID mice under anesthesia. For injection, the cells were resuspended in a 1:1 mixture of medium and Matrigel (BD Biosciences). The HuH7 cell–xenografted mice were treated with 5-FU (30 mg/kg; intraperitoneal administration) or ubenimex (20 mg/kg; oral administration) for 3 days. On the following day, mice were sacrificed and tumors were enucleated for the immunohistochemical assay. In the studies of PLC/PRF/5 cell–xenografted mice, mice were treated with 5-FU (30 mg/kg, 5 days of intraperitoneal injection and 2 days of withdrawal, 2 courses; 14 days), ubenimex (20 mg/kg, 14 days of forced oral administration), or ubenimex and 5-FU (combination of 2 courses of 30 mg/kg of 5-FU and 14 days of 20 mg/kg of ubenimex). The tumor size was calculated as follows: tumor volume (mm^3) = $a \times b/2$, where a = long axis and b = short axis. The relative tumor volume was calculated as follows: relative tumor volume (%) = $a/b \times 100$, where a = tumor volume before treatment (mm^3) and b = tumor volume after 14 days of treatment. The day after 14 days of treatment, mice were sacrificed and tumors were enucleated for immunohistochemical assay. The relative tumor volume was estimated as follows: relative tumor volume (mm^3) = tumor volume on the day after 14 days of treatment (mm^3)/tumor volume just before the start of treatment (mm^3) × 100 (%). The residual tumors after 14 days of 5-FU treatment were enucleated and minced into 2-mm squares and subcutaneously transplanted into secondary NOD/SCID mice with Matrigel. The mice were treated with ubenimex (20 mg/kg) from the day after transplantation for 7 days. Tumor growth was observed for 3 weeks. We used 4 or more mice for each model to enable statistical assessment of the results. All animal studies were approved by the Animal Experiments Committee at Osaka University.

ROS assay. To study intracellular ROS levels, cells were loaded with 10 μM of DCF-DA at 37°C for 30 minutes. ROS was activated by treatment with 100 μM H_2O_2 at 37°C for 120 minutes. To study the effect of CD13 inhibition on ROS levels, cells were pretreated with 5 μg/ml of the CD13-neutralizing antibody or 25 μg/ml of ubenimex at 37°C for 4 hours and stained with DCF-DA. For mitochondria ROS detection, cells were loaded with 5 μM MitoSOX (Molecular Probes) at 37°C for 20 minutes.

DNA fragmentation assay. For the alkaline comet assay, 5,000 isolated cells were irradiated (4 Gy) on ice and suspended in 0.6% of low melting point agarose, spread over the wells of slides, and immersed in alkaline solution for 30 minutes using a kit (Trevigen). Alkaline electrophoresis was then performed. Slides were stained with silver for visualization. For the tempol experiments, cells were treated with 10 mM of tempol (Sigma-Aldrich) for 15 minutes before irradiation. For in situ hybridization detection of fragmented DNA, 10-μm-thick serial sections obtained from fresh frozen samples were hybridized with TdT using tumor TACS in situ apoptosis detection kit (Trevigen) according to the manufacturer's protocols.

To identify DNA double-strand breaks, Alexa Fluor 488 Mouse Anti-H2AX (BD Pharmingen) was used according to the manufacturer's protocols. Briefly, cells were irradiated at 4 Gy. Cells were incubated in culture medium at 37°C in a humidified atmosphere containing 5% CO_2 after irradiation for 0, 2, 4, and 6 hours. After incubation, cells were stained with cell-surface antibodies. Then cells were fixed and permeabilized using Cytofix/Cytoperm Fixation/Permeabilization Solution Kit (BD), and stained with Alexa Fluor 488 Mouse Anti-H2AX.

Statistics. We determined statistical significance by 1-tailed Student's *t* test. $P < 0.05$ was defined as significant.

Acknowledgments

We thank T. Shimooka for technical assistance in this study. This work was supported in part by a grant from the Core Research for Evolutional Science and Technology (CREST), a grant-in-aid for Scientific Research on Priority Areas (20012039), a grant-in-aid for Scientific Research (category S) (21229015), and a grant-in-aid for Young Scientists (category B) (21790274) from the Ministry of Education, Culture, Sports, Science, and Technology, Japan.

Received for publication February 3, 2010, and accepted in revised form June 30, 2010.

Address correspondence to: Masaki Mori, Department of Gastroenterological Surgery, Graduate School of Medicine, Osaka University, 2-2 Yamadaoka, Suita 565-0871, Japan. Phone: 81.6.6879.3251; Fax: 81.6.6879.3259; E-mail: mmori@gesurg.med.osaka-u.ac.jp.

1. Visvader JE, Lindeman GJ. Cancer stem cells in solid tumours: accumulating evidence and unresolved questions. *Nat Rev Cancer.* 2008;8(10):755–768.
2. Lapidot T, et al. A cell initiating human acute myeloid leukaemia after transplantation into SCID mice. *Nature.* 1994;367(6464):645–648.
3. Arai F, et al. Tie2/angiopoietin-1 signaling regulates hematopoietic stem cell quiescence in the bone marrow niche. *Cell.* 2004;118(2):149–161.
4. Guan Y, Gerhard B, Hogge DE. Detection, isolation, and stimulation of quiescent primitive leukemic progenitor cells from patients with acute myeloid leukemia (AML). *Blood.* 2003;101(8):3142–3149.
5. Holyoake T, Jiang X, Eaves C, Eaves A. Isolation of a highly quiescent subpopulation of primitive leukemic cells in chronic myeloid leukemia. *Blood.* 1999; 94(6):2056–2064.
6. Meng S, et al. Circulating tumor cells in patients with breast cancer dormancy. *Clin Cancer Res.* 2004; 10(24):8152–8162.
7. El-Serag HB, Rudolph KL. Hepatocellular carcinoma: epidemiology and molecular carcinogenesis. *Gastroenterology.* 2007;132(7):2557–2576.
8. Haraguchi N, et al. Characterization of a side population of cancer cells from human gastrointestinal system. *Stem Cells.* 2006;24(3):506–513.
9. Ma S, et al. Identification and characterization of tumorigenic liver cancer stem/progenitor cells. *Gastroenterology.* 2007;132(7):2542–2556.
10. Ding W, et al. CD133+ liver cancer stem cells from methionine adenosyl transferase 1A-deficient mice demonstrate resistance to transforming growth factor (TGF)-beta-induced apoptosis. *Hepatology.* 2009; 49(4):1277–1286.
11. Zhu Z, et al. Cancer stem/progenitor cells are highly enriched in CD133(+)CD44(+) population in hepatocellular carcinoma. *Int J Cancer.* 2009; 126(9):2067–2078.
12. Yang ZF, et al. Significance of CD90+ cancer stem

cells in human liver cancer. *Cancer Cell.* 2008; 13(2):153–166.
13. Yang ZF, et al. Identification of local and circulating cancer stem cells in human liver cancer. *Hepatology.* 2008;47(3):919–928.
14. Yamashita T, et al. EpCAM-positive hepatocellular carcinoma cells are tumor-initiating cells with stem/progenitor cell features. *Gastroenterology.* 2009;136(3):1012–1024.
15. Ashmun RA, Shapiro LH, Look AT. Deletion of the zinc-binding motif of CD13/aminopeptidase N molecules results in loss of epitopes that mediate binding of inhibitory antibodies. *Blood.* 1992; 79(12):3344–3349.
16. Look AT, Ashmun RA, Shapiro LH, Peiper SC. Human myeloid plasma membrane glycoprotein CD13 (gp150) is identical to aminopeptidase N. *J Clin Invest.* 1989;83(4):1299–1307.
17. Ashmun RA, Look AT. Metalloprotease activity of CD13/aminopeptidase N on the surface of human myeloid cells. *Blood.* 1990;75(2):462–469.
18. Nakamura H, Suda H, Takita T, Aoyagi T, Umezawa H. X-ray structure determination of (2S, 3R)-3-amino-2-hydroxy-4-phenylbutanoic acid, a new amino acid component of bestatin. *J Antibiot.* 1976; 29(1):102–103.
19. Mathé G. Bestatin, an aminopeptidase inhibitor with a multi-pharmacological function. *Biomed Pharmacother.* 1991;45(2–3):49–54.
20. Kobayashi T, et al. Randomized trials between behenoyl cytarabine and cytarabine in combination induction and consolidation therapy, and with or without ubenimex after maintenance/intensification therapy in adult acute myeloid leukemia. The Japan Leukemia Study Group. *J Clin Oncol.* 1996; 14(1):204–213.
21. Hadnagy A, Gaboury L, Beaulieu R, Balicki D. SP analysis may be used to identify cancer stem cell populations. *Exp Cell Res.* 2006;312(19):3701–3710.
22. Vander Borght S, et al. Expression of multidrug resistance-associated protein 1 in hepatocellular carcinoma is associated with a more aggressive tumour phenotype and may reflect a progenitor cell origin. *Liver Int.* 2008;28(10):1370–1380.
23. Kamiya A, Kakinuma S, Yamazaki Y, Nakauchi H. Enrichment and clonal culture of progenitor cells during mouse postnatal liver development in mice. *Gastroenterology.* 2009;137(3):1114–1126.
24. Kaluz S, Kaluzová M, Liao SY, Lerman M, Stanbridge EJ. Transcriptional control of the tumor- and hypoxia-marker carbonic anhydrase 9: A one transcription factor (HIF-1) show? *Biochim Biophys Acta.* 2009;1795(2):162–172.
25. Miyamoto K, et al. Foxo3a is essential for maintenance of the hematopoietic stem cell pool. *Cell Stem Cell.* 2007;1(1):101–112.
26. Moore KA, Lemischka IR. Stem cells and their niches. *Science.* 2006;311(5769):1880–1885.
27. Naka K, Muraguchi T, Hoshii T, Hirao A. Regulation of reactive oxygen species and genomic stability in hematopoietic stem cells. *Antioxid Redox Signal.* 2008;10(11):1883–1894.
28. Estrela JM, Ortega A, Obrador E. Glutathione in cancer biology and therapy. *Crit Rev Clin Lab Sci.* 2006; 43(2):143–181.
29. Riley P. Free radicals in biology: oxidative stress and the effects of ionizing radiation. *Int J Radiat Biol.* 1994; 65(1):27–33.
30. Chen HT, et al. Response to RAG-mediated VDJ cleavage by NBS1 and gamma-H2AX. *Science.* 2000; 290(5498):1962–1965.
31. Hashida H, et al. Aminopeptidase N is involved in cell motility and angiogenesis: its clinical significance in human colon cancer. *Gastroenterology.* 2002; 122(2):376–386.
32. Menrad A, Speicher D, Wacker J, Herlyn M. Biochemical and functional characterization of aminopeptidase N expressed by human melanoma cells. *Cancer Res.* 1993;53(6):1450–1455.
33. Mishima Y, et al. Leukemic cell-surface CD13/aminopeptidase N and resistance to apoptosis mediated by endothelial cells. *J Natl Cancer Inst.* 2002;94(13):1020–1028.
34. Petrovic N, et al. CD13/APN regulates endothelial invasion and filopodia formation. *Blood.* 2007; 110(1):142–150.
35. Aihara M, et al. A combined approach for purging multidrug-resistant leukemic cell lines in bone marrow using a monoclonal antibody and chemotherapy. *Blood.* 1991;77(9):2079–2084.
36. Fairchild CR, et al. Carcinogen-induced mdr overexpression is associated with xenobiotic resistance in rat preneoplastic liver nodules and hepatocellular carcinomas. *Proc Natl Acad Sci U S A.* 1987; 84(21):7701–7705.
37. Ito K, et al. Regulation of oxidative stress by ATM is required for self-renewal of haematopoietic stem cells. *Nature.* 2004;431(7011):997–1002.
38. Ito K, et al. Reactive oxygen species act through p38 MAPK to limit the lifespan of hematopoietic stem cells. *Nat Med.* 2006;12(4):446–451.
39. Diehn M, et al. Association of reactive oxygen species levels and radioresistance in cancer stem cells. *Nature.* 2009;458(7239):780–783.
40. Hosokawa K, et al. Function of oxidative stress in the regulation of hematopoietic stem cell-niche interaction. *Biochem Biophys Res Commun.* 2007; 363(3):578–583.

Research Article

EASL EUROPEAN ASSOCIATION FOR THE STUDY OF THE LIVER | JOURNAL OF HEPATOLOGY

The *let-7* family of microRNAs inhibits Bcl-xL expression and potentiates sorafenib-induced apoptosis in human hepatocellular carcinoma

Satoshi Shimizu[1,†], Tetsuo Takehara[1,†], Hayato Hikita[1], Takahiro Kodama[1], Takuya Miyagi[1], Atsushi Hosui[1], Tomohide Tatsumi[1], Hisashi Ishida[1], Takehiro Noda[2], Hiroaki Nagano[2], Yuichiro Doki[2], Masaki Mori[2], Norio Hayashi[1,*]

[1]*Department of Gastroenterology and Hepatology, Osaka University Graduate School of Medicine, 2-2 Yamada-oka, Suita, Osaka 565-0871, Japan;* [2]*Department of Surgery, Osaka University Graduate School of Medicine, Osaka, Japan*

Background & Aims: Bcl-xL, an anti-apoptotic member of the Bcl-2 family, is over-expressed in human hepatocellular carcinoma, conferring a survival advantage to tumour cells. The mechanisms underlying its dysregulation have not been clarified. In the present study, we explored the involvement of microRNAs that act as endogenous sequence-specific suppressors of gene expression.

Methods: The expression profiles of microRNAs in Huh7 hepatoma cells and primary human hepatocytes were compared by microarray analysis. The effect of *let-7* on Bcl-xL expression was examined by Western blot and a reporter assay. The involvement of *let-7* microRNAs in human tissues was analysed by western blot and reverse transcription-PCR.

Results: Microarray analysis, followed by *in silico* target prediction, identified *let-7* microRNAs as being downregulated in Huh7 hepatoma cells in comparison with primary human hepatocytes, as well as possessing a putative target site in the *bcl-xl* mRNA. Over-expression of *let-7c* or *let-7g* led to a clear decrease of Bcl-xL expression in Huh7 and HepG2 cell lines. Reporter assays revealed direct post-transcriptional regulation involving *let-7c* or *let-7g* and the 3′-untranslated region of *bcl-xl* mRNA. Human hepatocellular carcinoma tissues with low expression of *let-7c* displayed higher expression of Bcl-xL protein than those with high expression of *let-7c*, suggesting that low *let-7* microRNA expression contributes to Bcl-xL over-expression. Finally, expression of *let-7c* enhanced apoptosis of hepatoma cells upon exposure to sorafenib, which downregulates expression of another anti-apoptotic Bcl-2 protein, Mcl-1.

Conclusions: *let-7* microRNAs negatively regulate Bcl-xL expression in human hepatocellular carcinomas and induce apoptosis in cooperation with an anti-cancer drug targeting Mcl-1.

Cancer

Introduction

MicroRNAs (miRNAs), a novel class of non-coding, small RNAs, repress gene expression by binding to the 3′-untranslated region (3′UTR) of target messenger RNAs (mRNAs) [1]. More than 500 miRNAs have been identified in humans. Each miRNA is capable of modulating the expression of many mRNAs to which it binds by imperfect sequence complementarity, although only a limited number of targeted genes has been identified. Through its activity of gene silencing, miRNA functions in a variety of cellular processes, such as development, organ homeostasis, and cancer development and progression [2]. In the context of cancer development and progression, miRNAs targeting oncogenes function as tumour suppressors, whereas those targeting tumour suppressor genes serve as oncogenes [3]. Accumulating evidence has revealed the aberrant expression of miRNAs in human hepatocellular carcinoma (HCC) [4–6]. *miR-122a* has been reported to be downregulated in HCC, in turn, leading to upregulation of cyclin G1 [7]. On the other hand, recent reports have demonstrated that *miR-21* [8], *miR-221* [9], and *miR-224* [10] are upregulated in HCC, leading to downregulation of PTEN, CDK inhibitors, and API-5, respectively. Furthermore, the miRNA expression signature was reported to be related to the clinical outcome of patients with HCC [11,12]. Thus, miRNAs may play an important role in HCC development and progression by modulating a variety of gene expression and cellular processes.

Apoptosis resistance is an important characteristic of tumour cells, in addition to dysregulated proliferation and aberrant differentiation. Apoptosis is regulated by a fine balance of Bcl-2 family proteins, such as anti-apoptotic Bcl-xL and Mcl-1 and pro-apoptotic Bak and Bax. We previously demonstrated that Bcl-xL

Keywords: Liver; Mcl-1; Bcl-2; Tumour; Epigenetic.
Received 2 July 2009; received in revised form 17 November 2009; accepted 2 December 2009; available online 4 March 2010
*Corresponding author. Tel.: +81 6 6879 3621; fax: +81 6 6879 3629.
E-mail address: hayashin@gh.med.osaka-u.ac.jp (N. Hayashi).
†These authors contributed equally to this work and share first authorship.
Abbreviations: miRNA, microRNA; 3′UTR, 3′-untranslated region; mRNA, messenger RNA; HCC, hepatocellular carcinoma; CDK, cyclin-dependent kinase; DMEM, Dulbecco's modified Eagle medium; RT, reverse transcription; PCR, polymerase chain reaction; 7-AAD, 7-amino-actinomycin D; DMSO, dimethyl sulfoxide.

is over-expressed in one-third of human HCC and confers resistance to hepatoma cells toward a variety of apoptotic insults generated by serum starvation and *p53* activation [13]. Patients with Bcl-xL-overexpressing HCC were shown to have significantly shorter disease-free survival after surgery [14]. Recently, it was proposed that autophagy defect is another mechanism of the malignant phenotype of Bcl-xL-overexpressing HCC through interaction between Bcl-xL and Beclin1 [15]. The underlying mechanisms of Bcl-xL over-expression in HCC are not clearly understood. Several reports show that transcription factors such as NF-κB [16] and STAT3 [17] could upregulate Bcl-xL expression in hepatoma cells. In addition, hepatitis C virus-related proteins, such as core [18] and NS5A [19], could upregulate Bcl-xL at a transcriptional level. However, we noticed that Bcl-xL-overexpressing hepatocarcinoma tissues do not always display upregulation of *bcl-xl* mRNA [13]. This observation led us to examine the possibility that post-transcriptional regulation by miRNAs may be involved in Bcl-xL expression in human HCC.

In the present study, we demonstrate that *let-7* family miRNAs, a prototype of human miRNAs [20], negatively regulate Bcl-xL expression in human HCC. *let-7* miRNAs are downregulated in human hepatoma cells and tissues in association with enhanced expression of Bcl-xL. Over-expression of *let-7* miRNAs in hepatoma cells downregulates Bcl-xL in a *bcl-xl* 3′UTR sequence-specific manner and enhances apoptosis induced by sorafenib, a recently approved anti-cancer drug for HCC [21]. The present study demonstrates for the first time that *let-7* miRNAs directly target Bcl-xL and induce apoptosis in cooperation with an anti-cancer drug targeting Mcl-1 in HCC.

Materials and methods

miRNA target predictions

The algorithms miRanda (http://www.microrna.org/), Pictar (http://pictar.mdc-berlin.de/), and TargetScan (http://www.targetscan.org/) were used to predict miRNAs that could potentially bind to *bcl-xl* mRNA.

Cell lines and tissues

Primary human hepatocytes were obtained from ScienCell Research Laboratories (Carlsbad, CA) and cultured with the provided medium. Human hepatoma cell lines, Huh7 and HepG2, were cultured with Dulbecco's modified Eagle medium (DMEM) supplemented with 10% heat-inactivated foetal bovine serum (Sigma, St. Louis, MO). HCCs and adjacent non-tumour counterparts were obtained at the time of surgical resection. Written informed consent was obtained from each patient. All tissues were stored at −80 °C until the time of use.

RNA extractions

Total RNA including the miRNA fraction was isolated from cell lines and tissue samples using the miRNeasy Mini Kit (QIAGEN, Valencia, CA). After extraction, the quality of each RNA sample was checked using an Agilent 2100 Bioanalyzer (Agilent Technologies, Santa Clara, CA).

miRNA microarray analysis

RNA labelling and hybridisation were performed using a human miRNA microarray kit and a miRNA complete labelling and hybridisation kit (Agilent Technologies). After washing with Gene Expression Wash Buffer, the slides were scanned with an Agilent Microarray Scanner and analysed by GeneSpring GX software.

Western blot

Cells or tissues were lysed and Western blotted as previously described [22]. For immunodetection, the following antibodies were used: anti-Bcl-xL polyclonal antibody (Santa Cruz Biotechnology, Santa Cruz, CA), anti-Mcl-1 polyclonal antibody (Santa Cruz Biotechnology), anti-Bak polyclonal antibody (Millipore, Billerica, MA), anti-Bax polyclonal antibody (Cell Signaling Technology, Danvers, MA). Optical densities of bands in each blot were analysed using ImageJ 1.40 g (NIH, Bethesda, MD).

Real time reverse transcription (RT)-PCR assays for mature miRNAs

To quantify the expression of mature miRNA, we synthesised cDNA from 10 ng of RNA sample using the TaqMan MicroRNA Reverse Transcription Kit (Applied Biosystems, Foster City, CA). Quantitative PCR was performed with TaqMan MicroRNA Assays (Applied Biosystems) specific for *let-7c* (P/N 4373167) and *let-7g* (P/N 4395393). To normalise the expression levels of miRNAs, we used TaqMan MicroRNA Assays specific for RNU6B (P/N 4373381) as the endogenous control.

Real time RT-PCR assays for bcl-xl mRNA

We reverse-transcribed RNA with High Capacity RNA-to-cDNA Master Mix (Applied Biosystems), and *bcl-xl* mRNA expression was measured using TaqMan Gene Expression Assays (Applied Biosystems, Assay ID: Hs99999146_m1). We also quantified *β-actin* mRNA as an endogenous control (Assay ID: Hs99999903_m1).

Transfections with miRNAs

Huh7 and HepG2 cells were transfected with 50 nM Pre-miR miRNA precursor molecules (Ambion, Austin, TX) of either *let-7c* or *let-7g* using RNAiMAX (Invitrogen, Carlsbad, CA) in six-well plates according to the manufacturer's instructions. Pre-miR negative control (Ambion) was also used as a control.

Luciferase assay

To generate the pMIR-Bcl-xL-3′UTR construct that contains the putative binding site of *bcl-xl* 3′UTR downstream of the firefly luciferase gene, we synthesised oligonucleotides to mimic the target sequence and inserted them into the SpeI–HindIII site of pMIR-REPORT Luciferase vector (Ambion). We also generated a pMIR-Bcl-xL-3′UTR mutant that has a point mutation in the putative binding site, using the QuickChange Multi Site-Directed Mutagenesis Kit (Stratagene, La Jolla, CA).

Each of these constructs was transfected into Huh7 cells together with 50 nM Pre-miR miRNA precursor molecules and pMIR-REPORT β-Gal vector (Ambion), which contains the β-galactosidase gene for normalisation of transfection efficiency. Transfection was performed using Lipofectamine 2000 (Invitrogen). We measured firefly luciferase activity 24 h after transfection using the Luciferase Assay System (Promega, Madison, WI) and normalised it to the β-galactosidase expression level.

In vitro staurosporine or sorafenib treatment

Huh7 cells were transfected with 50 nM Pre-miR miRNA precursor molecules as described above, and 48 h after transfection, the medium was changed to DMEM containing staurosporine (Calbiochem, Gibbstown, NJ) or sorafenib. Sorafenib was kindly provided by Bayer HealthCare Pharmaceuticals Inc. (Wayne, NJ). Cells were additionally cultured and assayed for apoptosis by monitoring the activity of caspase-3/7 using a luminescent substrate assay for caspase-3 and caspase-7 (Caspase-Glo assay, Promega, Madison, WI), or by flow cytometry using the Annexin V-PE Apoptosis Detection Kit I (BD Biosciences, San Jose, CA). We defined apoptotic cells as Annexin V-PE-positive and 7-amino-actinomycin D (7-AAD)-negative cells. Cell viability was determined by the WST assay using cell count reagent SF (Nacalai Tesque, Kyoto, Japan).

Statistical analysis

Data are presented as mean ± SD. Comparisons between two groups were performed by the unpaired *t*-test. Multiple comparisons were performed by ANOVA with the Scheffe post hoc test. $p < 0.05$ was considered statistically significant.

Results

let-7 miRNAs were downregulated in hepatoma cells with upregulated expression of Bcl-xL

As observed in human HCC tissues, Bcl-xL was over-expressed, according to Western blot analysis, in Huh7 and HepG2 human hepatoma cell lines compared to normal hepatocytes (Fig. 1A). Previous research established that 30 and 32 kDa species are original and post-translationally modified Bcl-xL, respectively [23]. Mcl-1 was also over-expressed in human hepatoma cells, but the levels of expression of Bak and Bax did not differ between hepatoma cells and normal hepatocytes. We reasoned that miRNA regulating Bcl-xL expression would be downregulated in those hepatoma cell lines. To search for the candidate miRNA, microarray analysis was performed. More specifically, miRNA expression in Huh7 cells and normal hepatocytes was compared. When levels of expression less than 50% were considered significant, 26 miRNAs were identified as being downregulated in Huh7 cells: *let-7b, let-7g, let-7i, miR-127-3p, miR-214, miR-376a, miR-381, miR-409-3p, miR-376c, miR-493*, miR-432, miR-487b, let-7d, let-7a, let-7f, let-7c, miR-200a, let-7e, miR-134, miR-503, miR-34a, miR-638, miR-150*, miR-1225-5p, miR-21*,* and *miR-223.* Among them, *in silico* analysis revealed that only the *let-7* family is capable of potentially targeting the 3′UTR of the *bcl-xl* mRNA. To confirm the results of the microarray analysis, quantitative real time RT-PCR was performed to evaluate the expression of *let-7c* and *let-7g* (Fig. 1B). After normalisation to endogenous RNU6B expression levels, the expression levels of both miRNAs were substantially lower in Huh7 cells than in normal hepatocytes. These results were consistent with the results of microarray analysis. Furthermore, the expression levels of both miRNAs were found to be downregulated in another human hepatoma cell line, HepG2, compared to normal hepatocytes.

let-7c and let-7g downregulate Bcl-xL expression by directly targeting the 3′UTR of bcl-xl mRNA

To examine whether *let-7* miRNAs are capable of suppressing translation of Bcl-xL, hepatoma cell lines were transfected with *let-7c* or *let-7g* or the negative control. Three days after transfection, Huh7 cells showed a decrease in Bcl-xL protein levels in both the *let-7c*-transfected group and the *let-7g*-transfected group in comparison with the negative control group (Fig. 2A). The transfection of *let-7c* and *let-7g* showed suppression of Bcl-xL protein levels in HepG2 cells as well (Fig. 2B). It did not affect expression of Bak and Bax, but increased Mcl-1 expression, which may be a secondary phenomenon of suppression of Bcl-xL. Normal hepatocytes were also transfected with *let-7c* or *let-7g* (Suppl. Fig. 1). The transfection led to a decrease in Bcl-xL expression in normal hepatocytes, but the decline was lesser than that observed in hepatoma cells. This finding may be explained by the observation that endogenous expression of *let-7c* and *let-7g* was extremely high in normal hepatocytes.

To examine whether the downregulation of Bcl-xL by *let-7c* or *let-7g* is caused by direct binding to a putative targeting site in the *bcl-xl* mRNA, we constructed the luciferase reporter plasmid pMIR-Bcl-xL-3′UTR containing the putative *let-7* binding site of *bcl-xl* 3′UTR downstream of the luciferase open reading frame (Fig 3A). The pMIR-Bcl-xL-3′UTR construct was cotransfected with the control pMIR-REPORT β-gal vector into Huh7 cells together with *let-7c* or *let-7g* or the negative control. When *let-7c* or *let-7g* Pre-miR was cotransfected with pMIR-Bcl-xL-3′UTR, the expression of firefly luciferase was significantly reduced compared to the negative control cotransfected group. There was no difference in firefly luciferase expression levels when pMIR-REPORT, which does not contain the putative *let-7* binding site, was cotransfected with *let-7c*, *let-7g* or the negative control (Fig. 3B). We also generated a pMIR-Bcl-xL-3′UTR mutant with a single base mutation in the seed region of the putative binding sequence to investigate whether the downregulation of firefly luciferase can be attributed to the insert (Fig. 3A). A single base mutation prevented the downregulation of firefly luciferase

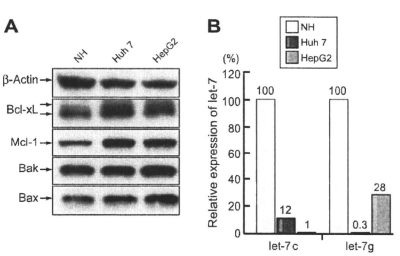

Fig. 1. Expression of Bcl-xL and *let-7* miRNAs in cultured human hepatocytes and hepatoma cells. Human hepatoma cell lines, Huh7 and HepG2, and normal hepatocytes (NH) were cultured and then lysed. (A) Western blot analysis for Bcl-2 family proteins. Bcl-xL migrates as a doublet band (see text). (B) Real time RT-PCR analysis for *let-7c* and *let-7g* expression. After normalisation to endogenous RNU6B expression, the expression of each miRNA in hepatoma cells was expressed in comparison to the levels observed in normal hepatocytes.

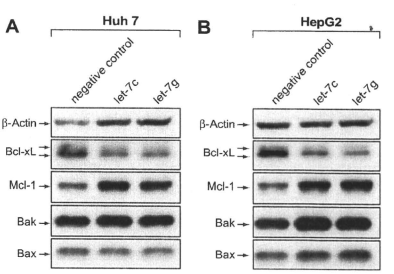

Fig. 2. Over-expression of *let-7* miRNAs downregulates Bcl-xL expression in hepatoma cells. Hepatoma cell lines Huh7 (A) and HepG2 (B) were transfected with *let-7c*, *let-7g*, or negative control miRNA at 50 nM and cultured for 3 days. Expression levels of Bcl-2 family proteins were determined by Western blot analysis.

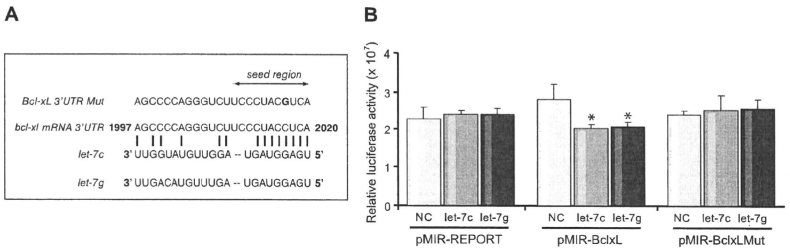

Fig. 3. Sequence-specific suppression of *bcl-xl* gene expression by *let-7c* or *let-7g* miRNAs. (A) The putative target site of *bcl-xl* mRNA 3'UTR determined by computational predictions. The target sequence was cloned into pMIR-REPORT vector (pMIR-Bcl-xL-3'UTR). pMIR-Bcl-xL-3'UTR mutant was also generated with a single mutation (indicated by a bold character) in the target site. (B) Each of these constructs was transfected into Huh7 cells together with *let-7c*, *let-7g* or negative control miRNA (NC). At 24 h after transfection, the activity of firefly luciferase was measured and normalised to β-galactosidase expression levels ($n = 3$). $^*p < 0.05$.

induced by *let-7c* or *let-7g*, which strongly suggests a direct inhibitory effect of *let-7* on Bcl-xL expression (Fig. 3B).

Downregulation of let-7c miRNA in human HCC tissues overexpressing Bcl-xL but not bcl-xl mRNA

To investigate the relationship between *let-7* expression levels and Bcl-xL protein levels in human HCC samples, we used 22 pairs of surgically resected human HCC tissue samples and adjacent non-tumour tissue samples with highly preserved RNA. Compared to the non-tumour counterparts, *bcl-xl* mRNA was found to be over-expressed in HCC tissue samples in only two cases; Bcl-xL was also over-expressed at the protein level in these cases. To assess the significance of *let-7* in post-transcriptional regulation of Bcl-xL *in vivo*, we selected 20 pairs of HCC tissue samples that did not over-express *bcl-xl* mRNA. When these samples were divided into two groups according to relative *let-7c* expression levels, the relative expression of Bcl-xL protein was significantly higher in the *let-7c* low expression group than in the *let-7c* high expression group (Fig. 4). By contrast, there was no significant difference in *bcl-xl* mRNA expression between the two groups. We also examined the relationship between relative *let-7g* expression and Bcl-xL expression. The *let-7g* low expression group tended to over-express Bcl-xL protein compared to the *let-7g* high expression group, although the difference did not reach statistical significance (data not shown). These results are consistent with the hypothesis that *let-7* miRNAs negatively regulate Bcl-xL expression independent of transcriptional regulation.

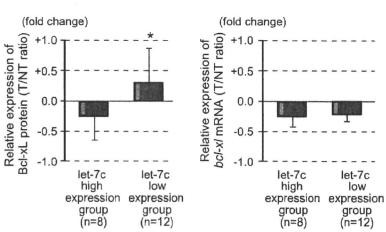

Fig. 4. Expression of Bcl-xL, *bcl-xl* mRNA and *let-7* miRNAs in human HCC tissue. Relationship between *let-7* and Bcl-xL expression in human HCC tissue samples. HCC tissue samples that did not show transcriptional upregulation of *bcl-xl* mRNA were divided into two groups according to relative *let-7c* expression levels with the threshold set at a 0.4-fold change in the tumour to non-tumour (T/NT) ratio. Relative expression of Bcl-xL protein and *bcl-xl* mRNA was calculated as the optical densities of the Bcl-xL blots normalised with the β-actin blots and those of real time RT-PCR assays, respectively, and are shown as the ratio of expression in the tumour to non-tumour expression in $\log_{10}$ scale. $^*p < 0.05$.

let-7c miRNA sensitises human Huh7 cells to sorafenib, which downregulates Mcl-1 expression

To investigate the effect of *let-7* in the resistance of hepatoma cells to apoptosis, we transfected Huh7 hepatoma cells with *let-7c* miRNAs and then subjected them to apoptosis analysis and a cell viability assay. There was no significant difference in caspase-3/7 activation or cell viability between *let-7c* miRNA-transfected Huh7 cells and control miRNA-transfected Huh7 cells (represented by the DMSO-treated group of Fig. 5A and B). These results are in agreement with our previous finding that anti-sense oligonucleotide-mediated knockdown of Bcl-xL sensitised hepatoma cells to apoptotic stimuli, such as serum starvation and *p53* activation, but did not induce apoptosis by itself [13]. Next, we exposed miRNA-transfected Huh7 cells to staurosporine, which is a well-established apoptosis inducer. Staurosporine treatment induced apoptosis, as determined by caspase-3/7 activation and decreased the viability of Huh7 cells by itself, but *let-7c* miRNA-transfected Huh7 cells were more susceptible to staurosporine treatment than control miRNA-transfected cells. *let-7c* miRNA-transfected Huh7 cells showed a significant decrease in cell viability, even upon exposure to low-dose of staurosporine at which control miRNA-transfected Huh7 did not show a significant difference in cell viability (Fig. 5B). In addition, the activation of caspase-3/7 was more intense in *let-7c* miRNA-transfected Huh7 cells than in control miRNA-transfected Huh7 cells (Fig. 5A). Thus, suppression of *let-7* expression leading to over-expression of Bcl-xL, may be a mechanism by which hepatoma cells resist apoptotic stimuli. While normal hepatocytes were more sensitive to staurosporine than hepatoma cells, transfection of *let-7* miRNA did not affect sensitivity to staurosporine

Cancer

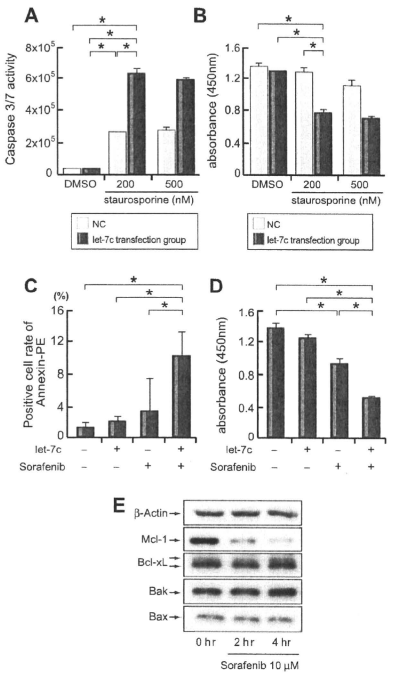

Fig. 5. Introduction of *let-7* miRNAs sensitises hepatoma cells to apoptotic stimuli. (A and B) Response to staurosporine treatment. Huh7 cells were transfected with *let-7c* (grey bars) or control miRNA (white bars) for 48 h and then further treated with staurosporine or DMSO alone for 12 h. The activities of caspase-3 and -7 were determined by luminescent substrate assays for caspase-3 and -7 ($n = 4$) (A). Cell viability was determined by the WST assay ($n = 4$) (B). *$p < 0.05$. (C and D) Response to sorafenib treatment. Huh7 cells were transfected with *let-7c* or control miRNA for 48 h and then further treated with sorafenib (5 μM) or DMSO alone for 48 h (C) or 72 h (D) 7-AAD negative cells were gated and the positive cell rate for annexin V-PE was determined ($n = 4$) (C). Cell viability was determined by the WST assay ($n = 4$) (D). *$p < 0.05$. E. Western blot analysis for Bcl-2 family proteins in lysates of Huh7 cells treated with sorafenib.

in normal hepatocytes (Suppl. Fig. 2), which is in agreement with the modest decline of Bcl-xL expression described earlier.

To examine the impact of *let-7* family miRNAs as a therapeutic tool, we investigated the effect of *let-7* miRNAs on apoptosis resistance to sorafenib, a recently approved anti-cancer drug for HCC. It has been reported that sorafenib was capable of downregulating Mcl-1 expression in tumour cells [24], and HCC has been reported to over-express Mcl-1, which is another anti-apoptotic Bcl-2 protein capable of conferring resistance to apoptosis [24–27]. In agreement with these findings, sorafenib treatment clearly downregulated Mcl-1 expression in hepatoma cells, but did not affect Bcl-xL expression (Fig. 5E). In contrast, sorafenib treatment did not affect Mcl-1 expression in normal hepatocytes (Suppl. Fig. 3). We hypothesised that *let-7* miRNA targeting Bcl-xL may induce apoptosis of hepatoma cells in cooperation with sorafenib. Apoptosis determined by Annexin V staining did not increase in *let-7c* miRNA-treated Huh7 cells compared to control miRNA-treated cells (represented by the DMSO-treated group in Fig. 5C). Sorafenib treatment of Huh7 cells led to a slight increase in the annexin V-positive cell rate, although the difference did not reach statistical significance levels under our experimental conditions (Fig. 5C). Of importance is the finding that sorafenib-induced apoptosis was markedly enhanced in *let-7c* miRNA-transfected cells. In addition, sorafenib treatment significantly reduced the viability of Huh7 cells and this decrease was markedly enhanced in cells transfected with *let-7c* miRNA (Fig. 5D). This finding implies that *let-7* miRNA transfection potentiates sorafenib-induced apoptosis and toxicity in hepatoma cells.

Discussion

Anti-apoptotic members of the Bcl-2 family, which consists of five members, Bcl-2, Bcl-xL, Mcl-1, Bcl-w, and Bfl-1, are critically involved in the mitochondrial pathway of apoptosis [28]. Cancer cells frequently over-express one or more members of this family to acquire a survival advantage [29]. These proteins are over-expressed in a variety of ways, including genetic translocation, particularly in the case of Bcl-2, and transcriptional regulation. Unlike the case of the *bcl-2* gene, mutations or amplification of the *bcl-x* gene have not been demonstrated in tumour cells. With regard to miRNA regulation, previous research clearly demonstrated that Bcl-2 is a direct target of *miR-15* and *miR-16*. The expression levels of *miR-15* and *miR-16* inversely correlate with Bcl-2 expression in chronic lymphocytic leukaemia [30]. More recently, Mcl-1 was reported to be suppressed by *miR-29* [31]. Our present study is the first demonstration of miRNA-mediated regulation of Bcl-xL expression. Since Bcl-xL is over-expressed not only in HCC but also in other tumours, the present findings may shed light on the mechanisms of Bcl-xL over-expression in other malignancies.

While more than 500 human miRNAs have been identified, *let-7* is a prototype of human miRNA and was first identified in 2001 [32]. *let-7* miRNAs are downregulated in several malignancies. A highly characterised example is non-small cell lung cancer in which downregulation of *let-7* miRNAs is well correlated with poor prognosis in patients [33]. In HCC, some reports showed downregulation of *let-7*, while others did not [7]. In the present study, *let-7c* miRNA was under-expressed at less than 40% of the normal level in approximately half of the HCC tissues. Further study is needed to determine the clinical significance of *let-7* miRNA in HCC. Several target genes have been identified for *let-7* miRNA, including Ras [34], Myc [35], HMGA2 [36], CDC25A, and CDK6 [37]. The major function of this miRNA is to promote cell proliferation. Since these proteins could act as oncogenes in tumour cells, *let-7* miRNA is believed to serve as a tumour suppressor [38]. In the present study, we have demonstrated that *bcl-xl* is a direct target for *let-7* miRNA, implying that this well-known tumour suppressor miRNA directly regulates apoptosis, another important process in malignancy.

Sorafenib is a recent FDA-approved anti-cancer drug for HCC [21]. It functions as a multi-kinase inhibitor and can induce

apoptosis at least in part by downregulating Mcl-1 in tumour cells [24]. Like Bcl-xL, several reports have identified Mcl-1 as being over-expressed in some HCCs [25–27]. Since Bcl-xL and Mcl-1 share a similar structure and functions, we reasoned that downregulation of both proteins would efficiently kill hepatoma cells. To verify this hypothesis, we treated hepatoma cells with sorafenib and *let-7* miRNA. As expected, sorafenib treatment downregulated Mcl-1 expression as early as 2 h post-treatment; however, it did not efficiently induce apoptosis. Transfection of *let-7* miRNA itself was not capable of inducing apoptosis of hepatoma cells despite a clear reduction in Bcl-xL expression. Importantly, *let-7* miRNA substantially increased sensitivity to sorafenib. Since both *let-7* miRNA and sorafenib may have pleiotropic effects on gene expression and cellular processes, downregulation of Bcl-xL and Mcl-1 may not be a single mechanism for killing hepatoma cells. However, our study revealed that Bcl-xL-targeting miRNA, *let-7*, controls resistance of hepatoma cells to this novel class of anti-HCC drug.

In conclusion, we have demonstrated that *let-7* miRNA negatively regulates Bcl-xL expression in HCCs. Reconstitution of *let-7* miRNA may reduce apoptosis resistance to anti-cancer drugs targeting Mcl-1 in HCC. Further study is needed to examine the significance of *let-7* miRNA expression for predicting responses to sorafenib therapy in patients with HCC.

Financial support

This work was partly supported by a Grant-in-Aid for Scientific Research from the Ministry of Education, Culture, Sports, Science and Technology, Japan (to T. Tak).

Disclosures

All authors have nothing to disclose.

Conflicts of interest

All authors have no conflicts of interest.

Acknowledgements

We thank Bayer HealthCare Pharmaceuticals Inc. (Wayne, NJ) for providing sorafenib.

Appendix A. Supplementary data

Supplementary data associated with this article can be found, in the online version, at doi:10.1016/j.jhep.2009.12.024.

References

[1] Filipowicz W, Bhattacharyya SN, Sonenberg N. Mechanisms of post-transcriptional regulation by microRNAs: are the answers in sight? Nat Rev Genet 2008;9:102–114.
[2] Esquela-Kerscher A, Slack FJ. Oncomirs – microRNAs with a role in cancer. Nat Rev Cancer 2006;6:259–269.
[3] Zhang B, Pan X, Cobb GP, Anderson TA. MicroRNAs as oncogenes and tumor suppressors. Dev Biol 2007;302:1–12.
[4] Murakami Y, Yasuda T, Saigo K, Urashima T, Toyoda H, Okanoue T, et al. Comprehensive analysis of microRNA expression patterns in hepatocellular carcinoma and non-tumorous tissues. Oncogene 2006;25:2537–2545.
[5] Varnholt H, Drebber U, Schulze F, Wedemeyer I, Schirmacher P, Dienes HP, et al. MicroRNA gene expression profile of hepatitis C virus-associated hepatocellular carcinoma. Hepatology 2008;47:1223–1232.
[6] Wong QW, Lung RW, Law PT, Lai PB, Chan KY, To KF, et al. MicroRNA-223 is commonly repressed in hepatocellular carcinoma and potentiates expression of Stathmin1. Gastroenterology 2008;135:257–269.
[7] Gramantieri L, Ferracin M, Fornari F, Veronese A, Sabbioni S, Liu CG, et al. Cyclin G1 is a target of miR-122a, a microRNA frequently downregulated in human hepatocellular carcinoma. Cancer Res 2007;67:6092–6099.
[8] Meng F, Henson R, Wehbe-Janek H, Ghoshal K, Jacob ST, Patel T. MicroRNA-21 regulates expression of the PTEN tumor suppressor gene in human hepatocellular cancer. Gastroenterology 2007;133:647–658.
[9] Fornari F, Gramantieri L, Ferracin M, Veronese A, Sabbioni S, Calin GA, et al. MiR-221 controls CDKN1C/p57 and CDKN1B/p27 expression in human hepatocellular carcinoma. Oncogene 2008;27:5651–5661.
[10] Wang Y, Lee AT, Ma JZ, Wang J, Ren J, Yang Y, et al. Profiling microRNA expression in hepatocellular carcinoma reveals microRNA-224 up-regulation and apoptosis inhibitor-5 as a microRNA-224-specific target. J Biol Chem 2008;283:13205–13215.
[11] Budhu A, Jia HL, Forgues M, Liu CG, Goldstein D, Lam A, et al. Identification of metastasis-related microRNAs in hepatocellular carcinoma. Hepatology 2008;47:897–907.
[12] Ladeiro Y, Couchy G, Balabaud C, Bioulac-Sage P, Pelletier L, Rebouissou S, et al. MicroRNA profiling in hepatocellular tumors is associated with clinical features and oncogene/tumor suppressor gene mutations. Hepatology 2008;47:1955–1963.
[13] Takehara T, Liu X, Fujimoto J, Friedman SL, Takahashi H. Expression and role of Bcl-xL in human hepatocellular carcinomas. Hepatology 2001;34:55–61.
[14] Watanabe J, Kushihata F, Honda K, Sugita A, Tateishi N, Mominoki K, et al. Prognostic significance of Bcl-xL in human hepatocellular carcinoma. Surgery 2004;135:604–612.
[15] Ding ZB, Shi YH, Zhou J, Qiu SJ, Xu Y, Dai Z, et al. Association of autophagy defect with a malignant phenotype and poor prognosis of hepatocellular carcinoma. Cancer Res 2008;68:9167–9175.
[16] Chiao PJ, Na R, Niu J, Sclabas GM, Dong Q, Curley SA. Role of Rel/NF-kappaB transcription factors in apoptosis of human hepatocellular carcinoma cells. Cancer 2002;95:1696–1705.
[17] Selvendiran K, Koga H, Ueno T, Yoshida T, Maeyama M, Torimura T, et al. Luteolin promotes degradation in signal transducer and activator of transcription 3 in human hepatoma cells: an implication for the antitumor potential of flavonoids. Cancer Res 2006;66:4826–4834.
[18] Otsuka M, Kato N, Taniguchi H, Yoshida H, Goto T, Shiratori Y, et al. Hepatitis C virus core protein inhibits apoptosis via enhanced Bcl-xL expression. Virology 2002;296:84–93.
[19] Sarcar B, Ghosh AK, Steele R, Ray R, Ray RB. Hepatitis C virus NS5A mediated STAT3 activation requires co-operation of Jak1 kinase. Virology 2004;322:51–60.
[20] Pasquinelli AE, Reinhart BJ, Slack F, Martindale MQ, Kuroda MI, Maller B, et al. Conservation of the sequence and temporal expression of let-7 heterochronic regulatory RNA. Nature 2000;408:86–89.
[21] Llovet JM, Bruix J. Molecular targeted therapies in hepatocellular carcinoma. Hepatology 2008;48:1312–1327.
[22] Takehara T, Tatsumi T, Suzuki T, Rucker 3rd EB, Hennighausen L, Jinushi M, et al. Hepatocyte-specific disruption of Bcl-xL leads to continuous hepatocyte apoptosis and liver fibrotic responses. Gastroenterology 2004;127:1189–1197.
[23] Takehara T, Takahashi H. Suppression of Bcl-xL deamidation in human hepatocellular carcinomas. Cancer Res 2003;63:3054–3057.
[24] Rahmani M, Davis EM, Bauer C, Dent P, Grant S. Apoptosis induced by the kinase inhibitor BAY 43-9006 in human leukemia cells involves down-regulation of Mcl-1 through inhibition of translation. J Biol Chem 2005;280:35217–35227.
[25] Sieghart W, Losert D, Strommer S, Cejka D, Schmid K, Rasoul-Rockenschaub S, et al. Mcl-1 overexpression in hepatocellular carcinoma: a potential target for antisense therapy. J Hepatol 2006;44:151–157.
[26] Fleischer B, Schulze-Bergkamen H, Schuchmann M, Weber A, Biesterfeld S, Müller M, et al. Mcl-1 is an anti-apoptotic factor for human hepatocellular carcinoma. Int J Oncol 2006;28:25–32.
[27] Schulze-Bergkamen H, Fleischer B, Schuchmann M, Weber A, Weinmann A, Krammer PH, et al. Suppression of Mcl-1 via RNA interference sensitizes human hepatocellular carcinoma cells towards apoptosis induction. BMC Cancer 2006;6:232.
[28] Youle RJ, Strasser A. The BCL-2 protein family: opposing activities that mediate cell death. Nat Rev Mol Cell Biol 2008;9:47–59.

[29] Lessene G, Czabotar PE, Colman PM. BCL-2 family antagonists for cancer therapy. Nat Rev Drug Discov 2008;7:989–1000.
[30] Cimmino A, Calin GA, Fabbri M, Iorio MV, Ferracin M, Shimizu M, et al. MiR-15 and miR-16 induce apoptosis by targeting BCL2. Proc Natl Acad Sci USA 2005;102:13944–13949.
[31] Mott JL, Kobayashi S, Bronk SF, Gores GJ. Mir-29 regulates Mcl-1 protein expression and apoptosis. Oncogene 2007;26:6133–6140.
[32] Lagos-Quintana M, Rauhut R, Lendeckel W, Tuschl T. Identification of novel genes coding for small expressed RNAs. Science 2001;294:853–858.
[33] Takamizawa J, Konishi H, Yanagisawa K, Tomida S, Osada H, Endoh H, et al. Reduced expression of the let-7 microRNAs in human lung cancers in association with shortened postoperative survival. Cancer Res 2004;64:3753–3756.
[34] Johnson SM, Grosshans H, Shingara J, Byrom M, Jarvis R, Cheng A, et al. RAS is regulated by let-7 microRNA family. Cell 2005;120:635–647.
[35] Sampson VB, Rong NH, Han J, Yang Q, Aris V, Soteropoulos P, et al. MicroRNA let-7a down-regulates MYC and reverts MYC-induced growth in Burkitt lymphoma cells. Cancer Res 2007;67:9762–9770.
[36] Lee YS, Dutta A. The tumor suppressor microRNA let-7 represses the HMGA2 oncogenes. Genes Dev 2007;21:1025–1030.
[37] Johnson CD, Esquela-Kerscher A, Stefani G, Byrom M, Kelnar K, Ovcharenko D, et al. The let-7 microRNA represses cell proliferation pathways in human cells. Cancer Res 2007;67:7713–7722.
[38] Büssing I, Slack FJ, Grosshans H. let-7 microRNAs in development, stem cells and cancer. Trend Mol Med 2008;14:400–409.

Ann Surg Oncol (2010) 17:967–972
DOI 10.1245/s10434-009-0865-y

Annals of
SURGICAL ONCOLOGY
OFFICIAL JOURNAL OF THE SOCIETY OF SURGICAL ONCOLOGY

ORIGINAL ARTICLE – COLORECTAL CANCER

TGM2 Is a Novel Marker for Prognosis and Therapeutic Target in Colorectal Cancer

Norikatsu Miyoshi, MD[1], Hideshi Ishii, MD[1,2], Koshi Mimori, MD[2], Fumiaki Tanaka, MD[2], Toshiki Hitora, MD[1], Mitsuyoshi Tei, MD[1], Mitsugu Sekimoto, MD[1], Yuichiro Doki, MD, PhD[1], and Masaki Mori, MD, PhD, FACS[1]

[1]Department of Gastroenterological Surgery, Osaka University Graduate School of Medicine, Osaka, Japan; [2]Division of Molecular and Surgical Oncology, Department of Molecular and Cellular Biology, Medical Institute of Bioregulation, Kyushu University, Ohita, Japan

ABSTRACT

Background. Transglutaminase 2 (*TGM2*) plays a role in cell growth and survival through the antiapoptosis signaling pathway.

Methods. We analyzed *TGM2* gene expression in 91 paired cases of colorectal cancer (CRC) and noncancerous regions and seven CRC cell lines to demonstrate the importance of *TGM2* expression for the prediction of prognosis of CRC. *TGM2* expression was higher in CRC tissue than in corresponding normal tissue by real-time reverse transcriptase–polymerase chain reaction ($P = .015$).

Results. Patients in the high *TGM2* expression group showed a poorer overall survival rate than those in the low expression group ($P = .001$), indicating that the increase in *TGM2* expression was an independent prognostic factor. *TGM2* was also expressed in the seven CRC cell lines. The in vitro proliferation assay showed that *TGM2* expression is involved with tumor growth.

Conclusions. The present study suggests that *TGM2* is useful as a predictive marker for patient prognosis and may be a novel therapeutic target for CRC.

Cancer is a major public health problem in developed countries, while the incidence of colorectal cancer (CRC) has greatly increased in Japan in recent years as a result of lifestyle changes.[1] CRC is now one of the most important causes of death from neoplastic disease in Japan.[1] Therefore, identification of the genes responsible for the development and progression of CRC and understanding the clinical significance are critical for the diagnosis and adequate treatment of the disease.

Transglutaminase 2, *TGM2*, is a family of enzymes that catalyzes the formation of an amide bond between the γ-carboxamide groups of peptide-bound glutamine residues and the primary amino groups in various compounds.[2,3] Several studies have reported that that increased expression of *TGM2* indicates prolonged cell survival and the prevention of apoptosis.[4–9]

We analyzed *TGM2* in seven human gastrointestinal cancer cell lines and 91 paired cases of CRC and noncancerous regions to identify the importance of *TGM2* expression for prognosis and to suggest that it be a candidate novel marker for the prognosis with functional relevance in CRCs.

MATERIALS AND METHODS

Clinical Tissue Samples

From 1992 to 2002, 91 patients (62 men, 29 women) with CRC underwent surgery at the Medical Institute of Bioregulation at Kyusyu University. Primary CRC specimens and adjacent normal colorectal mucosa were obtained from patients after receiving informed consent in accordance with the institutional guidelines. Every patient was definitively identified with CRC on the basis of clinicopathological findings. Tissues were extracted immediately after surgical resections. The specimens were immediately fixed in formalin, processed through graded ethanol,

Electronic supplementary material The online version of this article (doi:10.1245/s10434-009-0865-y) contains supplementary material, which is available to authorized users.

First Received: 20 July 2009;
Published Online: 22 December 2009

M. Mori, MD, PhD, FACS
e-mail: mmori@gesurg.med.osaka-u.ac.jp

embedded in paraffin, and sectioned with hematoxylin and eosin stain and elastica van Gieson stain, and the degree of the histological differentiation, lymphatic invasion, and venous invasion was examined. All specimens were frozen in liquid nitrogen immediately after resection and stored at −80°C until RNA extractions were performed.

None of the patients received chemotherapy or radiotherapy before surgery. After the surgery, the patients were followed up with a blood examination that included the tumor markers carcinoembryonic antigen and cancer antigen, and imaging modalities such as abdominal ultrasound, computed tomography, and chest x-ray every 3 to 6 months. Clinicopathological factors were assessed according to the criteria of the tumor node metastasis classification of the International Union Against Cancer.[10]

Cell Lines and Culture

Seven cell lines derived from human CRC (Caco2, DLD-1, HCT116, HT-29, KM12SM, LoVo, and SW480) were obtained and maintained in Dulbecco modified Eagle medium containing 10% fetal bovine serum and antibiotics at 37°C in a 5% humidified CO_2 atmosphere. For the siRNA knockdown experiment, double-stranded RNA duplexes targeting human *TGM2* (5′-UAGGAUCCCAUCUUCAA ACUGCCCA-3′/5′-UGGGCAGUUUGAAGAUGGGAUC CUA-3′, 5′-AUCCCAUUGUAGCUGACGGUGCGGG-3′/ 5′-CCCGCACCGUGAGCUACAAUGGGAU-3′, and 5′-UG UAGUUGGUCACGACGCGGGUAGG-3′/5′-CCUACCCG CGUCGUGACCAACUACA-3′) were purchased (Stealth RNAi) from Invitrogen (Carlsbad, CA). Negative control siRNA (NC) was also purchased from Invitrogen. CRC cell lines were transfected with siRNA at a concentration of 20 μmol/L with lipofectamine (RNAiMAX, Invitrogen), incubated in glucose-free Opti-MEM (Invitrogen) for the time indicated, and analyzed by the proliferation assay. All siRNA duplexes were used together as a triple transfection. siRNA knockdowns were performed in seven CRC cell lines to evaluate proliferation under *TGM2* suppression. Each cell line with siRNA was compared with the negative control. The values are presented as mean ± standard deviation (SD) from independent experiments conducted in triplicate.

RNA Preparation and Quantitative Real-Time Reverse Transcriptase–Polymerase Chain Reaction

Total RNA was prepared by using a modified acid guanidium-phenol-chloroform procedure with DNase.[11] Reverse transcription was performed from 2.5 μg of total RNA as previously described.[12] A 143-bp *TGM2* fragment was amplified. Two human *TGM2* oligonucleotide primers for the polymerase chain reaction (PCR) reaction were designed as follows: 5′-ATAAGTTAGCGCCGCTCTCC-3′ (forward); 5′-CCAGCTCCAGATCACACCTC-3′ (reverse). The forward primer is located in exon 1 and the reverse primer in exon 2. The PCR assay with primers specific to the glyceraldehyde-3-phosphate dehydrogenase (*GAPDH*) gene was performed to evaluate expression. The *GAPDH* primers, 5′-TTGGTATCGTGGAAGGACTCA-3′ (forward) and 5′-TGTCATCATATTGGCAGGTT-3′ (reverse), produced a 270-bp amplicon. cDNA from the Human Reference Total RNA (Clontech, Palo Alto, CA) was studied concurrently as a positive control. Real-time monitoring of the PCRs was performed with the LightCycler FastStart DNA Master SYBR Green I kit (Roche Diagnostics, Tokyo, Japan) for cDNA amplification of *TGM2* and *GAPDH*. The amplification protocol consisted of 35 cycles of denaturation at 95°C for 10 seconds, annealing at 60°C for 10 seconds, and elongation at 72°C for 10 seconds. The products were then subjected to a temperature gradient from 55°C to 95°C at 0.1°C per second with continuous fluorescence monitoring to produce product melting curves. The expression ratio of mRNA copies in tumor and normal tissues was calculated and normalized against *GAPDH* mRNA expression.

Proliferation Assays

In CRC cell lines transfected with siRNA, 1×10^5 cells were seeded in 12-well dishes and cultured for 96 hours to determine proliferation. The cell growth rate was measured by counting cells with a CellTac kit (Nihon Koden, Tokyo, Japan).

Statistical Analysis

Continuous variable data were expressed as mean ± SD. The relationship between mRNA expression and clinicopathological factors were analyzed by the χ^2 test and Student's *t*-test. Kaplan-Meier survival curves were plotted and compared with the generalized log rank test. Univariate and multivariate analyses to identify prognostic factors for overall survival were performed by the Cox proportional hazard regression model. All tests were analyzed by JMP software (SAS Institute, Cary, NC). *P* values of <.05 were considered statistically significant.

RESULTS

TGM2 mRNA Expression in Clinical Tissue Specimens

Reverse transcriptase–polymerase chain reaction (RT-PCR) of 91 paired clinical samples showed that 65 (71.4%) of the 91 cases exhibited higher levels of *TGM2* mRNA in tumors than paired normal tissues (Fig. 1). The mean *TGM2* mRNA expression value in tumor tissues was

significantly higher than that for corresponding normal tissues ($P = .015$; Student's *t*-test).

TGM2 Expression and Clinicopathological Characteristics

The experimental samples were divided into two groups according to expression status for the clinicopathological evaluation. Patients with tumors that had more than the median *TGM2/GAPDH* expression (median .329) were assigned to the high expression group ($n = 46$); the others were assigned to the low expression group ($n = 45$, Table 1). The number of cases that were based on histological grade was 37, 47, 4, and 3 in the well, moderate, poor, and mucinous adenocarcinoma categories, respectively. *TGM2* expression was correlated with tumor type ($P = .002$), tumor invasion ($P < .001$), lymph node metastasis ($P = .041$), lymphatic invasion ($P = .010$), metastasis ($P = .040$), and International Union Against Cancer stage ($P < .001$).

Relationship Between TGM2 Expression and Prognosis

Postoperative overall survival rate was statistically significantly lower in patients with increased *TGM2* expression (Fig. 2). The median follow-up was 4.12 years. Table 2 provides the univariate and multivariate analyses of factors related to patient prognosis. Univariate analysis showed that histological grade ($P = .040$), tumor type ($P = .003$), tumor size ($P = .004$), tumor invasion

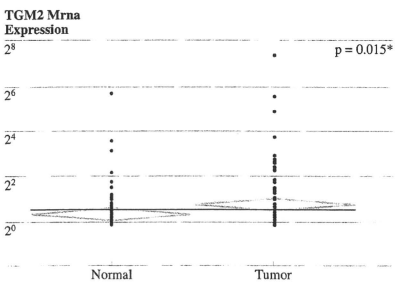

FIG. 1 Transglutaminase 2 (*TGM2*) mRNA expression in clinical tissue specimens. Quantitative real-time reverse transcriptase–polymerase chain reaction of 91 paired clinical samples showed that 65 (71.4%) of the 91 cases exhibited higher levels of *TGM2* mRNA in tumors than in paired normal tissues. The mean *TGM2* mRNA expression in tumor tissues (normalized by *GAPDH* gene expression) was significantly higher than that of the corresponding normal tissues ($P = .015$; Student's *t*-test)

TABLE 1 Clinicopathological factors and TGM2 mRNA expression in 91 colorectal cancers

Factor	High expression ($n = 46$)	Low expression ($n = 45$)	*P* value
Age (y)			
<68	25 (54.3%)	17 (37.8%)	.112
≥68	21 (45.7%)	28 (62.2%)	
Sex			
Male	31 (67.4%)	31 (68.9%)	.878
Female	15 (32.6%)	14 (31.1%)	
Histological grade			
Wel/Mod	41 (89.1%)	43 (95.6%)	.242
Others	5 (10.9%)	2 (4.4%)	
Tumor type			
0–2	0–2 3 (6.5%)	14 (31.1%)	.002*
3–4	3–4 43 (93.5%)	31 (68.9%)	
Tumor size			
<30 mm	39 (84.8%)	35 (77.8%)	.391
≥30 mm	7 (15.2%)	10 (22.2%)	
Tumor invasion			
Tis	0 (0%)	5 (11.1%)	≤.001*
T1	2 (4.3%)	6 (13.3%)	
T2	3 (6.5%)	12 (26.7%)	
T3	28 (60.9%)	18 (40.0%)	
T4	13 (28.3%)	4 (8.9%)	
Lymph node metastasis			
N0	22 (47.8%)	31 (68.9%)	.041*
N1–2	24 (52.2%)	14 (31.1%)	
Lymphatic invasion			
Absent	24 (52.2%)	35 (77.8%)	.010*
Present	22 (47.8%)	10 (22.2%)	
Venous invasion			
Absent	38 (82.6%)	40 (88.9%)	.392
Present	8 (17.4%)	5 (11.1%)	
Metastasis			
M0	29 (63.0%)	37 (82.2%)	.040*
M1	17 (37.0%)	8 (17.8%)	
UICC stage			
0	0 (0%)	5 (11.1%)	≤.001*
I	5 (10.9%)	12 (26.7%)	
IIA	11 (23.9%)	11 (24.4%)	
IIB	2 (4.3%)	1 (2.2%)	
IIIA	0 (0%)	5 (11.1%)	
IIIB	8 (17.4%)	3 (6.7%)	
IIIC	3 (6.5%)	0 (0%)	
IV	17 (37.0%)	8 (17.8%)	

Wel well differentiated adenocarcinoma, *mod* moderately differentiated adenocarcinoma, *others* poorly differentiated adenocarcinoma and mucinous carcinoma, *UICC* International Union Against Cancer

* Statistically significant

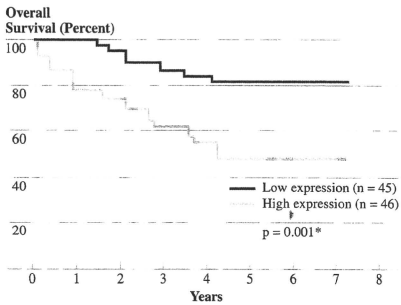

FIG. 2 Overall survival curves of colorectal cancer patients based on *TGM2* mRNA expression status. The postoperative overall survival rate was significantly lower among patients in the high *TGM2* expression group ($P = .001$, log rank test) than the low expression group. The median follow-up was 4.12 years

($P < .001$), lymph node metastasis ($P < .001$), lymphatic invasion ($P = .006$), venous invasion ($P = .001$), and *TGM2* mRNA expression ($P = .003$) were significantly related to overall survival. Multivariate analysis indicated that inclusion in the *TGM2* mRNA high expression group (relative risk, 2.40; 95% confidence interval, 1.03–6.11; $P = .041$) was an independent predictor of postoperative overall survival, as was metastasis (M1/M0, relative risk, 5.86; 95% confidence interval, 2.49–15.12; $P < .001$).

In Vitro Assessment of TGM2 Expression Knockdown

Seven CRC cell lines were used for the proliferation study because *TGM2* expression was higher than the median value of *GAPDH* in the primary CRC specimen by RT-PCR. A reduction in *TGM2* by siRNA was observed by quantitative real-time RT-PCR in all the cell lines examined (negative control [NC] and *TGM2* siRNAs; $P < .05$, Student's *t*-test). A reduction in *TGM2* expression was confirmed in the HT-29, HCT116, KM12SM, and LoVo cell lines (Suppl. Fig. S1). In proliferation assay, there were differences in cell numbers of HT-29 between NC and *TGM2* siRNA ($P < .05$) (Fig. 3). There was no statistically significant difference in the number between the NC and *TGM2* siRNA in the other cell lines.

DISCUSSION

Previous reports showed that *TGM2*, also known as *TG2*, is expressed in breast and pancreatic cancer cells and is associated with drug resistance and metastasis.[4–16] *TGM2* promotes a stable interaction with extracellular matrix protein components in association with some β members of the integrin family of proteins, which induce cell survival signaling pathways.[17] Other reports suggest that *TGM2* regulates activation of NF-κB by forming a ternary complex with NF-κB/IκBα, and inhibition of apoptosis through transamidation and GTP-binding activity.[4,9,18]

Seven distinct transglutaminases have been described.[19–22] *TGM2* is ubiquitously expressed as a single/polypeptide protein that exhibits Ca^{2+}-dependent protein cross-linking activity.[23]

We assessed *TGM2* gene expression and found that it was a statistically significant independent prognostic factor, similar to the well-known important predictive factor.[24] To our knowledge, the present study is the first report

TABLE 2 Univariate and multivariate analyses for overall survival (Cox proportional hazard regression model)

Factor	Univariate analysis			Multivariate analysis		
	RR	95% CI	*P* value	RR	95% CI	*P* value
Age (y), <68/≥68	1.47	0.70–3.11	.298			
Sex, male/female	1.40	0.64–3.38	.401			
Histological grade, por–others/well–mod	3.66	1.06–9.64	.040*	2.52	0.68–7.45	.148
Tumor type, 3–4/0–2	8.27	1.76–147.44	.003*	1.80	0.22–40.49	.615
Tumor size, ≥30 cm/<30 cm	2.82	1.30–11.91	.004*	1.26	0.45–6.02	.697
Tumor invasion, T3–4/Tis-2	7.60	2.27–47.16	≤.001*	1.13	0.36–2.68	.802
Lymph node metastasis, N1–2/N0	5.42	2.43–13.74	≤.001*	2.06	0.83–5.74	.119
Lymphatic invasion, present/absent	2.80	1.34–5.89	.006*	1.32	0.53–3.22	.532
Venous invasion, present/absent	4.20	1.81–9.03	.001*	2.24	0.85–5.80	.099
Metastasis, M1/M0	8.93	4.14–20.84	≤.001*	5.86	2.49–15.12	≤.001*
TGM2 mRNA expression, ≥median/median>	3.08	1.43–7.18	.003*	2.40	1.03–6.11	.041*

RR relative risk, *95% CI* 95% confidence interva, *wel* well-differentiated adenocarcinoma, *mod* moderately differentiated adenocarcinoma, *por* poorly differentiated adenocarcinoma, *others* poorly differentiated adenocarcinoma and mucinous carcinoma

* Statistically significant

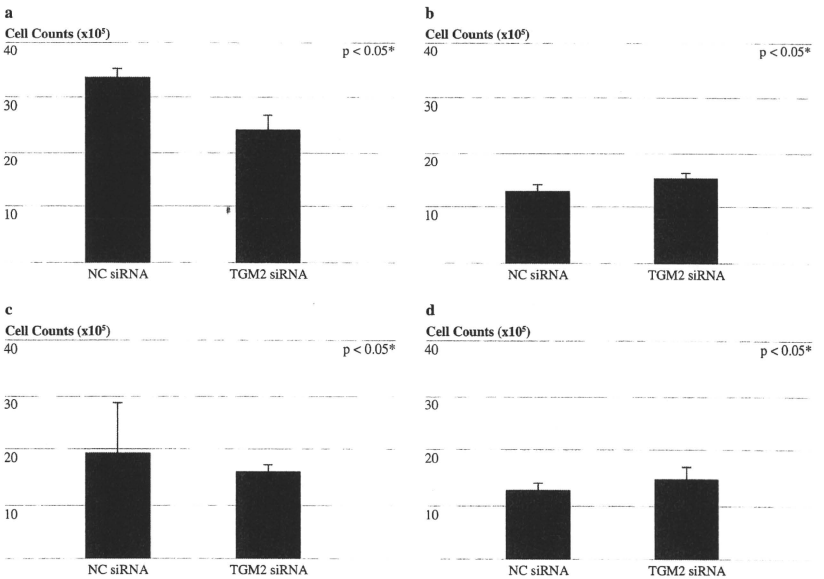

FIG. 3 Proliferation assay and siRNA inhibition in 4 colorectal cancer cell lines. The proliferation assay showed a difference in growth of colorectal cancer cell line HT-29. There were significant differences between NC and *TGM2* siRNA. In the other 3 cell lines, there was no significant difference between NC and *TGM2* siRNA (**a** HT-29; **b** HCT116; **c** KM12SM; **d** LoVo). Values are mean ± SD for three independent experiments. WT, wild type; NC, negative control

showing that *TGM2* is upregulated in CRCs, suggesting that it could be a novel predictive marker for the prognosis of CRCs that may contribute to further clinical cancer diagnosis.

Recently, the necessity of intensive follow-up and adjuvant therapy for CRC has been proposed to predict recurrence and metastasis in curative surgical resected cases.[25–27] In addition, there have been many recent reports on the use of less invasive surgery for CRC such as laparoscopic and endoscopic surgery.[28–31] For these cases, a predictive marker of tumor invasion, lymph node metastasis, and distant metastasis would play a very important role in cancer diagnoses and treatments, especially as a novel marker independent from the traditional tumor, node, metastasis factors. Thus, the *TGM2* expression profile could contribute to the predictive diagnosis of CRCs.

TGM2 plays an important role in antiapoptotic signaling pathways and several cancer cell lines that exhibit high *TGM2* expression levels and have been selected for resistance to chemotherapeutic drugs.[17,32,33] Downregulation of *TGM2* expression by siRNA rendered the cancer cells sensitive to chemotherapeutic drugs.[17]

The present in vitro study showed that *TGM2* expression is associated with tumor growth, and the inhibition of *TGM2* may lead to a reduction in CRC proliferation. *TGM2* is expressed in several cancers.[14–16] Our results suggest a rationale for further study of *TGM2* as a possible novel target for clinical cancer therapy such as anticancer agents and the sensitizer in addition to the novel marker of prognosis and prediction about the susceptibility of anticancer agents.

REFERENCES

1. Kohno SI, Luo C, Nawa A, et al. Oncolytic virotherapy with an HSV amplicon vector expressing granulocyte-macrophage colony-stimulating factor using the replication-competent HSV type 1 mutant HF10 as a helper virus. *Cancer Gene Ther.* 2007;14: 918–26.
2. Folk JE. Transglutaminases. *Annu Rev Biochem.* 1980;49: 517–31.

3. Lorand L, Graham RM. Transglutaminases: crosslinking enzymes with pleiotropic functions. *Nat Rev Mol Cell Biol.* 2003; 4:140–56.
4. Antonyak MA, Singh US, Lee DA, et al. Effects of tissue transglutaminase on retinoic acid–induced cellular differentiation and protection against apoptosis. *J Biol Chem.* 2001;276:33582–7.
5. Boehm JE, Singh U, Combs C, et al. Tissue transglutaminase protects against apoptosis by modifying the tumor suppressor protein p110 Rb. *J Biol Chem.* 2002;277:20127–30.
6. Antonyak MA, Miller AM, Jansen JM, et al. Augmentation of tissue transglutaminase expression and activation by epidermal growth factor inhibit doxorubicin-induced apoptosis in human breast cancer cells. *J BiolrChem.* 2004;279:41461–7.
7. Mangala LS, Mehta K. Tissue transglutaminase (TG2) in cancer biology. *Prog Exp Tumor Res.* 2005;38:125–38.
8. Mehta K. Mammalian transglutaminases: a family portrait. *Prog Exp Tumor Res.* 2005;38:1–18.
9. Mann AP, Verma A, Sethi G, et al. Overexpression of tissue transglutaminase leads to constitutive activation of nuclear factor-kappaB in cancer cells: delineation of a novel pathway. *Cancer Res.* 2006;66:8788–95.
10. Sobin LH, Fleming ID. TNM classification of malignant tumors, 5th edn. Union Internationale Contre le Cancer and the American Joint Committee on Cancer. *Cancer.* 1997;80:1803–4.
11. Mimori K, Mori M, Shiraishi T, et al. Clinical significance of tissue inhibitor of metalloproteinase expression in gastric carcinoma. *Br J Cancer.* 1997;76:531–6.
12. Mori M, Staniunas RJ, Barnard GF, et al. The significance of carbonic anhydrase expression in human colorectal cancer. *Gastroenterology.* 1993;105:820–6.
13. Fesus L, Piacentini M. Transglutaminase 2: an enigmatic enzyme with diverse functions. *Trends Biochem Sci.* 2002;27:534–9.
14. Mehta K. High levels of transglutaminase expression in doxorubicin-resistant human breast carcinoma cells. *Int J Cancer.* 1994;58:400–6.
15. Chen JS, Konopleva M, Andreeff M, et al. Drug-resistant breast carcinoma (MCF-7) cells are paradoxically sensitive to apoptosis. *J Cell Physiol.* 2004;200:223–34.
16. Mehta K, Fok J, Miller FR, et al. Prognostic significance of tissue transglutaminase in drug resistant and metastatic breast cancer. *Clin Cancer Res.* 2004;10:8068–76.
17. Herman JF, Mangala LS, Mehta K. Implications of increased tissue transglutaminase (TG2) expression in drug-resistant breast cancer (MCF-7) cells. *Oncogene.* 2006;25:3049–58.
18. Sarang Z, Molnar P, Nemeth T, et al. Tissue transglutaminase (TG2) acting as G protein protects hepatocytes against Fas-mediated cell death in mice. *Hepatology.* 2005;42:578–87.
19. Aeschlimann D, Paulsson M. Transglutaminases: protein cross-linking enzymes in tissues and body fluids. *Thromb Haemost.* 1994;71:402–15.
20. Aeschlimann D, Koeller MK, Allen-Hoffmann BL, Mosher DF. Isolation of a cDNA encoding a novel member of the transglutaminase gene family from human keratinocytes. Detection and identification of transglutaminase gene products based on reverse transcription–polymerase chain reaction with degenerate primers. *J Biol Chem.* 1998;273:3452–60.
21. Chen JS, Mehta K. Tissue transglutaminase: an enzyme with a split personality. *Int J Biochem Cell Biol.* 1999;31:817–36.
22. Greenberg CS, Birckbichler PJ, Rice RH. Transglutaminases: multifunctional cross-linking enzymes that stabilize tissues. *FASEB J.* 1991;5:3071–7.
23. Ai L, Kim WJ, Demircan B, et al. The transglutaminase 2 gene (*TGM2.*), a potential molecular marker for chemotherapeutic drug sensitivity, is epigenetically silenced in breast cancer. *Carcinogenesis.* 2008;29:510–8.
24. Andre T, Quinaux E, Louvet C, et al. Phase III study comparing a semimonthly with a monthly regimen of fluorouracil and leucovorin as adjuvant treatment for stage II and III colon cancer patients: final results of GERCOR C96.1. *J Clin Oncol.* 2007;25: 3732–8.
25. Wolpin BM, Mayer RJ. Systemic treatment of colorectal cancer. *Gastroenterology.* 2008;134:1296–10.
26. Kornmann M, Formentini A, Ette C, et al. Prognostic factors influencing the survival of patients with colon cancer receiving adjuvant 5-FU treatment. *Eur J Surg Oncol.* 2008;34:1316–21.
27. Bathe OF, Dowden S, Sutherland F, et al. 2004 Phase II study of neoadjuvant 5-FU + leucovorin + CPT-11 in patients with resectable liver metastases from colorectal adenocarcinoma. *BMC Cancer.* 4:32.
28. Lacy AM, Garcia-Valdecasas JC, Delgado S, et al. Laparoscopy-assisted colectomy versus open colectomy for treatment of non-metastatic colon cancer: a randomised trial. *Lancet.* 2002;359: 2224–9.
29. Weeks JC, Nelson H, Gelber S, et al. Short-term quality-of-life outcomes following laparoscopic-assisted colectomy vs open colectomy for colon cancer: a randomized trial. *JAMA.* 2002;287: 321–8.
30. Group COoSTS. 2004 A comparison of laparoscopically assisted and open colectomy for colon cancer. *N Engl J Med.* 350:2050–9.
31. Jayne DG, Guillou PJ, Thorpe H, et al. Randomized trial of laparoscopic-assisted resection of colorectal carcinoma: 3-year results of the UK MRC CLASICC Trial Group. *J Clin Oncol.* 2007;25:3061–8.
32. Han JA, Park SC. Reduction of transglutaminase 2 expression is associated with an induction of drug sensitivity in the PC-14 human lung cancer cell line. *J Cancer Res Clin Oncol.* 1999;125: 89–95.
33. Devarajan E, Chen J, Multani AS, et al. Human breast cancer MCF-7 cell line contains inherently drug-resistant subclones with distinct genotypic and phenotypic features. *Int J Oncol.* 2002;20:913–20.

Ann Surg Oncol (2010) 17:2526–2533
DOI 10.1245/s10434-010-1041-0

Annals of
SURGICAL ONCOLOGY
OFFICIAL JOURNAL OF THE SOCIETY OF SURGICAL ONCOLOGY

ORIGINAL ARTICLE – TRANSLATIONAL RESEARCH AND BIOMARKERS

The Clinical Significance of Vimentin-Expressing Gastric Cancer Cells in Bone Marrow

Masaaki Iwatsuki, MD[1,2], Koshi Mimori, MD[1], Takeo Fukagawa, MD[3], Hideshi Ishii, MD[1], Takehiko Yokobori, MD[1], Mitsuru Sasako, MD[3], Hideo Baba, MD[2], and Masaki Mori, MD, FACS[1]

[1]Department of Surgical Oncology, Medical Institute of Bioregulation, Kyushu University, Beppu, Japan; [2]Department of Gastroenterological Surgery, Graduate School of Medical Sciences, Kumamoto University, Kumamoto, Japan; [3]Gastric Surgery Division, National Cancer Center Hospital, Tokyo, Japan

ABSTRACT

Background. Expression of the mesenchymal marker gene vimentin (*VIM*) in gastric cancer is associated with a more aggressive form of the disease and poor prognosis. Because epithelial mesenchymal transition (EMT) plays a critical role in the progression of gastric cancer, *VIM* expression was examined in the bone marrow (BM) of gastric cancer patients.

Methods. BM samples from 437 gastric cancer patients were collected and analyzed by quantitative RT-PCR. Expression of VIM protein in the primary lesions of resected gastric cancers was evaluated using immunohistochemistry. Furthermore, induction of *VIM* expression by TGF-β1 and hypoxia was evaluated in gastric cancer cells.

Results. *VIM* mRNA expression increased concordantly with clinical staging and was significantly associated with tumor invasion and lymph node metastasis ($P < .0001$). Though cancer cells in the primary lesions did not stain with VIM antibody, some of the cells invading the intratumoral vessels were strongly positive for VIM, but were negative for E-cadherin. Hypoxic conditions and treatment with TGF-β1 induced *VIM* expression and repressed E-cadherin in gastric cancer cells, coupled with an alteration of cellular morphology.

Conclusions. We found that gastric cancer cells undergo EMT in BM to survive and metastasize. These findings suggest that isolated tumor cells have the potential to undergo EMT, which could increase the malignancy of gastric cancer.

Electronic supplementary material The online version of this article (doi:10.1245/s10434-010-1041-0) contains supplementary material, which is available to authorized users.

First Received: 23 June 2009;
Published Online: 1 April 2010

M. Mori, MD, FACS
e-mail: mmori@gesurg.med.osaka-u.ac.jp

Vimentin (VIM) expression has been reported in a variety of carcinomas, such as kidney, breast, lung, and thyroid.[1–4] Utsunomiya et al.[5] reported the significance of VIM expression in solid, poorly differentiated gastric adenocarcinomas, showing that the prognosis of VIM-expressing cases was poorer compared with that of VIM-negative cases. VIM is the predominant intermediate filament protein in mesenchymal cells and is not usually expressed by epithelial cells. Several previous studies indicate that VIM expression induces invasive behavior in human epithelial carcinoma cell lines.[6–8]

Recently, attention has focused on the role of EMT in cancer progression.[9] During epithelial mesenchymal transition (EMT), epithelial cell-cell adhesion is decreased by the downregulation of adhesion molecules such as E-cadherin, and cell morphology becomes fibroblastlike with upregulation of *VIM*.[10] EMT promotes cellular motility, invasiveness, and cytoskeletal rearrangement in a range of cancer cell lines.[11] Furthermore, several studies revealed that transcriptional repressors of E-cadherin such as zinc finger proteins (ZEB1, ZEB2), bHLH protein (twist), and the snail family of zinc finger protein (snail, slug) are associated with EMT.[12–16] Thus, they are useful markers to predict prognosis in various human carcinomas.[17–19] In addition, Kim et al.[20] demonstrated that the expression of EMT-related genes such as E-cadherin, vimentin, N-cadherin, and snail were associated with poor prognosis in gastric cancer.